Langevin-dynamics study of the dynamical properties of small magnetic particles

José Luis García-Palacios* and Francisco J. Lázaro
Instituto de Ciencia de Materiales de Aragón, Consejo Superior de Investigaciones Científicas-Universidad de Zaragoza, 50015 Zaragoza, Spain
(Received 3 March 1998; revised manuscript received 17 August 1998)

The stochastic Landau-Lifshitz-Gilbert equation of motion for a classical magnetic moment is numerically solved (properly observing the customary interpretation of it as a *Stratonovich stochastic differential equation*), in order to study the dynamics of magnetic nanoparticles. The corresponding Langevin-dynamics approach allows for the study of the fluctuating trajectories of individual magnetic moments, where we have encountered remarkable phenomena in the overbarrier rotation process, such as crossing-back or multiple crossing of the potential barrier, rooted in the gyromagnetic nature of the system. Concerning averaged quantities, we study the linear dynamic response of the archetypal ensemble of noninteracting classical magnetic moments with axially symmetric magnetic anisotropy. The results are compared with different analytical expressions used to model the relaxation of nanoparticle ensembles, assessing their accuracy. It has been found that, among a number of heuristic expressions for the linear dynamic susceptibility, only the simple formula *proposed* by Shliomis and Stepanov matches the coarse features of the susceptibility reasonably. By comparing the numerical results with the *asymptotic* formula of Storonkin {Sov. Phys. Crystallogr. **30**, 489 (1985) [Kristallografiya **30**, 841 (1985)]}, the effects of the intra-potential-well relaxation modes on the low-temperature longitudinal dynamic response have been assessed, showing their relatively small reflection in the susceptibility curves but their dramatic influence on the phase shifts. Comparison of the numerical results with the *exact* zero-damping expression for the transverse susceptibility by Garanin, Ishchenko, and Panina {Theor. Math. Phys. (USSR) **82**, 169 (1990) [Teor. Mat. Fiz. **82**, 242 (1990)]}, reveals a sizable contribution of the spread of the precession frequencies of the magnetic moment in the anisotropy field to the dynamic response at intermediate-to-high temperatures. [S0163-1829(98)00446-9]

I. INTRODUCTION

Magnetically ordered particles of nanometric size generally consist of a single domain, whose constituent spins, at temperatures well below the Curie temperature, rotate in unison. The magnetic energy of a nanometric particle is then determined by its magnetic moment orientation, and has a number of stable directions separated by potential barriers (associated with the magnetic anisotropy). As a result of the coupling of the magnetic moment of the particle, $\vec{m}$, with the microscopic degrees of freedom of its environment (phonons, conducting electrons, nuclear spins, etc.), the magnetic moment is subjected to thermal fluctuations and may undergo a Brownian-type rotation, surmounting the potential barriers. This solid-state relaxation process was proposed by Néel in the late 1940's,[1] and subsequently reexamined by Brown,[2] by means of the theory of stochastic processes (cf. Ref. 3).

In the high potential-barrier range, $\Delta U/k_{\mathrm{B}}T \gg 1$, the characteristic time for the overbarrier rotation process $\tau_{\parallel}$ can approximately be written in the Arrhenius form $\tau_{\parallel} \simeq \tau_0 \exp(\Delta U/k_{\mathrm{B}}T)$, where $\tau_0 (\sim 10^{-10}$–10^{-12} s) is related to the intra-potential-well dynamics. For $\tau_{\parallel} \ll t_{\mathrm{m}}$ (t_{m} is the measurement or observation time), $\vec{m}$ maintains the equilibrium distribution of orientations as in a classical paramagnet; as $m = |\vec{m}|$ is much larger than a typical microscopic magnetic moment ($m \sim 10^3$–10^5 μ_{B}) this phenomenon is named *superparamagnetism*. On the contrary, when $\tau_{\parallel} \gg t_{\mathrm{m}}$, $\vec{m}$ rotates rapidly about a potential minimum and the overbarrier relaxation mechanism is *blocked*. Finally, under intermediate conditions, *nonequilibrium phenomena*, accompanied by magnetic ''relaxation,'' are observed. It is to be noted that, in the Arrhenius range mentioned, the system may pass through all these regimes in a relatively narrow temperature interval.

In order to study the properties of classical magnetic moments, numerical simulation techniques can be used, with most of the studies that have been performed being based on the Monte Carlo method. Although this method is a rigorous and efficient tool to compute thermal-equilibrium quantities, the interpretation of the dynamical properties derived by means of Monte Carlo techniques, especially for non-Ising spins, is not free from criticism.[4,5] On the contrary, when using stochastic methods based on Fokker-Planck or Langevin equations, time does not merely label the sequential order of generated states when sampling the phase space, but is related to physical time.

For classical spins, the basic Langevin equation is the stochastic Landau-Lifshitz-Gilbert equation introduced by Brown[2] (see also Ref. 3). The *multiplicative* fluctuating terms occurring in this Langevin equation (see Sec. II) were treated in Brown's work, as well as in the subsequent theoretical developments, by means of the *Stratonovich stochastic calculus*. In this context, Brown constructed the celebrated Fokker-Planck (diffusion) equation for the time evolution of the nonequilibrium probability distribution of magnetic moment orientations. (If one uses the alternative *Itô stochastic calculus* to treat the multiplicative fluctuating terms, Brown's Fokker-Planck equation and hence all the results derived from it—relaxation times, dynamic suscepti-

bilities, etc.—should be altered.) In order to solve Brown's Fokker-Planck equation (which is a partial differential equation of parabolic type) a number of techniques have been used, such as direct solution techniques[6] or more elaborate approaches involving continued-fractions techniques or the numerical calculation of the eigenvalues and amplitudes of the relevant dynamical modes.[7–11]

An approach equivalent to solving a Fokker-Planck equation is to construct solutions of the underlying stochastic equation of motion of the system. This *Langevin-dynamics* approach bypasses the Fokker-Planck equation as it directly generates the stochastic trajectories of the variables of the system, from which averages can be computed. This is a relevant point since the solution of the Fokker-Planck equation for multivariate systems, either numerically or analytically, is usually a formidable task.

Lyberatos, Berkov, and Chantrell[12] developed a rigorous method, in the context of the Langevin-dynamics formalism for linear systems, for the numerical modeling of *small* thermal fluctuations in micromagnetic systems (linearized stochastic Landau-Lifshitz-Gilbert equation). Subsequently, Lyberatos and Chantrell[13] employed a generalization of this method to accommodate *large* fluctuations (a generalization that is equivalent to Brown approach; see Ref. 2, p. 1681). Unfortunately, in the corresponding numerical integration of the stochastic Landau-Lifshitz-Gilbert equation, care was not taken with the treatment of the aforementioned multiplicative fluctuating terms when choosing the numerical integration scheme. The method employed (a bare Euler scheme; see Appendix C) converges to an Itô solution of the stochastic differential equation. This fact, together with the relation between the temperature and the amplitude of the fluctuating terms used, which is essentially that derived from Brown's Fokker-Planck equation (Stratonovich calculus), renders the approach of Lyberatos and Chantrell inconsistent.

In this article, we shall integrate the stochastic Landau-Lifshitz-Gilbert equation numerically in the context of the Stratonovich stochastic calculus, by means of a judicious choice of the numerical integration scheme. This is undertaken taking account of the underlying subtleties of the stochastic calculus as compared with the deterministic calculus.

As the Langevin-dynamics method employed generates the self-same stochastic trajectories of each individual magnetic moment, it provides much insight into the dynamics of the system. In addition, the theoretical study of single-particle phenomena is of special interest because dynamical measurements of *individual* magnetic *nano*particles have recently been performed.[14]

In the study of individual trajectories, we shall find striking phenomena in the overbarrier rotation process—crossing-back and multiple crossing of the potential barrier, having their origins in the gyromagnetic nature of the system, are frequently encountered. The first suggestion of the former process goes back to Brown[15] in his lucid criticism of the calculation of Néel[1] of the relaxation time in terms of the rate of potential-barrier crossings of the magnetic moment. Here, this and related phenomena will be numerically verified.

Concerning the response of an ensemble of classical magnetic moments (averaged quantities), the Langevin-dynamics method allows the computation of any desired quantity, e.g., hysteresis loops, field-cooled and zero-field-cooled magnetization curves, relaxation times, linear and nonlinear susceptibilities, magnetic specific heat, and, with appropriate relationships between line shapes and correlation functions of the system, even spectroscopic quantities. We shall restrict our study to the linear dynamic response of the archetypal model for the nanoparticle system—an ensemble of noninteracting classical magnetic moments with axially symmetric magnetic anisotropy, dispersed in a solid nonmagnetic matrix. The linear dynamic response is chosen since it is a probe that allows one to examine the intrinsic dynamics of the system.

We shall investigate the effects of the intra-potential-well relaxation modes on the longitudinal dynamic response as well as the contribution of the spread of the precession frequencies of the magnetic moment in the anisotropy field to the transverse response. In addition, because some relevant parameters of nanoparticle ensembles can be extracted from the analysis of the dynamic-response data,[16,17] we shall assess the accuracy of the heuristic models employed in such analyses.

The organization of this article is as follows. In Sec. II the Brown-Kubo-Hashitsume model for the stochastic dynamics of classical magnetic moments is discussed. The results of the numerical integration of the stochastic Landau-Lifshitz-Gilbert equation are presented in Secs. III and IV (the numerical method is discussed in Appendix C). Specifically, Sec. III is devoted to the study of the trajectories of individual magnetic moments, while the dynamics of the spin ensemble is studied in Sec. IV. Some concluding remarks are finally given in Sec. V.

II. BROWN-KUBO-HASHITSUME STOCHASTIC MODEL

The description of the dynamics of a classical spin via the introduction of a Langevin equation was done by Brown,[2] in the context of the small-particle magnetism, and by Kubo and Hashitsume,[3] who studied generic classical spins. The developments based on each of these approaches have taken place separately in the literature. Nevertheless, both approaches are essentially equivalent and we shall present here a unified discussion of them.

A. Dynamical equations

1. Stochastic Landau-Lifshitz-Gilbert equation

In the Brown-Kubo-Hashitsume model the starting equation of motion for a classical magnetic moment $\vec{m}$ is the stochastic Gilbert equation[2,3] cast into the archetypal Landau-Lifshitz form. The resulting equation will be called the *stochastic Landau-Lifshitz-Gilbert equation*, and reads

$$\frac{d\vec{m}}{dt}=\gamma\vec{m}\wedge[\vec{B}_{\rm eff}+\vec{b}_{\rm fl}(t)]-\gamma\frac{\lambda}{m}\vec{m}\wedge\{\vec{m}\wedge[\vec{B}_{\rm eff}+\vec{b}_{\rm fl}(t)]\}, \tag{2.1}$$

where γ is a gyromagnetic ratio and λ is a dimensionless damping coefficient that measures the magnitude of the relaxation (damping) term relative to the gyromagnetic term in the dynamical equation. (For magnetic nanoparticles $\lambda=\eta\gamma m/v$ with η being the damping coefficient in the equa-

tion of Gilbert for the magnetization and v the volume of the nanoparticle.) We have not introduced the customary renormalized gyromagnetic ratio $\gamma/(1+\lambda^2)$ since one can alternatively consider Eq. (2.1) as the starting equation; if one wishes to consider the Gilbert form as the commencing equation, one just needs to substitute $\gamma \rightarrow \gamma/(1+\lambda^2)$ throughout.

In Eq. (2.1), the (deterministic) *effective field* is given by

$$\vec{B}_{\rm eff} = -\frac{\partial \mathcal{H}}{\partial \vec{m}}, \tag{2.2}$$

where $\mathcal{H}(\vec{m})$ is the Hamiltonian of the classical magnetic moment and $\partial/\partial\vec{m}$ stands for the gradient operator $[\partial f/\partial \vec{m} = (\partial f/\partial m_x)\hat{x} + (\partial f/\partial m_y)\hat{y} + (\partial f/\partial m_z)\hat{z}]$. For $\mathcal{H} = -\vec{m}\cdot\vec{B}$, one indeed has $\vec{B}_{\rm eff} = \vec{B}$ (this was the case thoroughly studied by Kubo and Hashitsume), whereas, in a more general situation, $\vec{B}_{\rm eff}$ incorporates the (deterministic) effects of the magnetic-anisotropy energy, the interaction with other spins, etc., on the dynamics of $\vec{m}$.

On the other hand, in Eq. (2.1), $\vec{B}_{\rm eff}$ has been augmented by a *fluctuating or stochastic field* $\vec{b}_{\rm fl}(t)$, accounting for the effects of the interaction of $\vec{m}$ with the microscopic degrees of freedom (phonons, conducting electrons, nuclear spins, etc.), which cause fluctuations of the magnetic moment orientation. Those environmental degrees of freedom are also responsible for the damped precession of $\vec{m}$, since fluctuations and dissipation are related manifestations of one and the same interaction of the magnetic moment with its environment.

The customary assumptions about $\vec{b}_{\rm fl}(t)$ are that it is a Gaussian stochastic process with the following statistical properties

$$\langle b_{{\rm fl},i}(t)\rangle = 0, \quad \langle b_{{\rm fl},i}(t) b_{{\rm fl},j}(s)\rangle = 2D\delta_{ij}\delta(t-s) \tag{2.3}$$

(recall that the first two moments determine a Gaussian process), where i and j are Cartesian indices, the constant D measures the strength of the thermal fluctuations (assumed isotropic), and $\langle\ \rangle$ denotes an average taken over different *realizations* of the fluctuating field. (The constant D is determined on the grounds of statistical-mechanical considerations; see below.) The Gaussian property of the fluctuations arises because they emerge from the interaction of $\vec{m}$ with a large number of microscopic degrees of freedom with equivalent statistical properties (central limit theorem). The Dirac δ in the second Eq. (2.3) expresses that above certain temperature the autocorrelation time of $\vec{b}_{\rm fl}(t)$ (of microscopic scale) is much shorter than the rotational-response time of the system (''white'' noise), while the Kronecker δ expresses that the different components of $\vec{b}_{\rm fl}(t)$ are assumed to be uncorrelated. Finally, it is also customarily assumed that the fluctuating fields acting on different magnetic moments are independent.

2. Stochastic Landau-Lifshitz equation

As will be shown below, the thermodynamic consistency of the approach entails $|\vec{b}_{\rm fl}| \sim \lambda^{1/2}$. Therefore, for weak damping ($\lambda \ll 1$) we can drop the fluctuating field from the relaxation term of Eq. (2.1), to arrive at

$$\frac{d\vec{m}}{dt} = \gamma\vec{m}\wedge[\vec{B}_{\rm eff} + \vec{b}_{\rm fl}(t)] - \gamma\frac{\lambda}{m}\vec{m}\wedge(\vec{m}\wedge\vec{B}_{\rm eff}). \tag{2.4}$$

This equation, which was indeed the equation studied by Kubo and Hashitsume,[3] will be called the *stochastic Landau-Lifshitz equation*. This is a Langevin equation more archetypal than Eq. (2.1), because the fluctuating and relaxation terms are not entangled.

On the other hand, one can bypass the reasoning employed to obtain Eq. (2.4) from Eq. (2.1), and consider the former as an alternative stochastic model. It will be shown below that, when the condition of thermodynamic consistency is applied, the *average* properties derived from both Eqs. (2.1) and (2.4) are completely equivalent.

3. The multiplicative noise terms

Apparently, for a given D, Eqs. (2.1) or (2.4), supplemented by Eqs. (2.3), fully determine the dynamical problem under consideration. Nevertheless, due to the vector *products* of $\vec{m}$ and $\vec{b}_{\rm fl}(t)$ occurring in those equations, the fluctuating field $\vec{b}_{\rm fl}(t)$ enters in a *multiplicative* way. This gives rise to some formal problems because, for white multiplicative noise, *any Langevin equation must be supplemented by an interpretation rule to properly define it* (Ref. 18, p. 246). Two dominant interpretations, which lead to either the Itô or the Stratonovich *stochastic calculus*, are usually considered, yielding different dynamical properties for the system. For instance, depending on the stochastic calculus used, disparate Fokker-Planck equations for the time evolution of the nonequilibrium probability distribution of the corresponding variables, are obtained. (For fluctuations with finite autocorrelation time or, for additive fluctuations, no ambiguity occurs and the mentioned stochastic calculi are equivalent.) The Itô calculus is commonly chosen on certain mathematical grounds, since rather general results of probability theory can then be employed. On the other hand, as the white noise is an idealization of physical noise with short autocorrelation time, the Stratonovich calculus is usually preferred in physical applications, since the associated results coincide with those obtained in the formal zero-correlation-time limit of fluctuations with finite autocorrelation time (see, e.g., Ref. 19). *Both the seminal works of Brown[2] and Kubo and Hashitsume,[3] as well as all the subsequent theoretical developments, are based, implicitly or explicitly, on the Stratonovich stochastic calculus.*

B. Fokker-Planck equation

The Fokker-Planck equation governing the time evolution of the nonequilibrium probability distribution of magnetic moment orientations associated with the stochastic Landau-Lifshitz-Gilbert equation (2.1) was originally derived by Brown.[2] By a different method and starting from the stochastic Landau-Lifshitz equation (2.4), Kubo and Hashitsume[3] arrived at an equation for the probability distribution, which, when the autocorrelation times of $\vec{b}_{\rm fl}(t)$ are much shorter than the precession period of $\vec{m}$, coincides with the Fokker-

Planck equation of Brown in the absence of the anisotropy potential (recall that they considered $\vec{B}_{\rm eff}=\vec{B}$). In Appendix B we give an alternative and simple derivation of the Fokker-Planck equations associated with Eqs. (2.1) and (2.4), showing that *both equations lead to Fokker-Planck equations that are structurally the same*.

Thus, on introducing the appropriate *Néel time* $\tau_{\rm N}$ [Eq. (B8)], which is the characteristic time of diffusion in the absence of potential (free-diffusion time; see below), the Fokker-Planck equations associated with Eqs. (2.1) and (2.4) can be written in a unified way as (cf. Ref. 20)

$$\frac{\partial P}{\partial t}=-\frac{\partial}{\partial \vec{m}}\cdot\left\{\left[\gamma\vec{m}\wedge\vec{B}_{\rm eff}-\gamma\frac{\lambda}{m}\vec{m}\wedge(\vec{m}\wedge\vec{B}_{\rm eff})+\frac{1}{2\tau_{\rm N}}\vec{m}\wedge\left(\vec{m}\wedge\frac{\partial}{\partial\vec{m}}\right)\right]P\right\}, \tag{2.5}$$

where $P(\vec{m},t)$ is the nonequilibrium probability distribution for $\vec{m}$ at time t, and $\partial/\partial\vec{m}\cdot$ stands for the divergence operator $[(\partial/\partial\vec{m})\cdot\vec{A}=\Sigma_i(\partial A_i/\partial m_i)]$.

1. Stationary solution

In order to ensure that the stationary properties of the system derived from Eqs. (2.1) or (2.4), supplemented by Eqs. (2.3), coincide with the appropriate thermal-equilibrium properties, the Fokker-Planck equation associated with these Langevin equations is forced to have the Boltzmann distribution

$$P_0(\vec{m})\propto\exp[-\beta\mathcal{H}(\vec{m})]$$

as a stationary solution. To do so, note first that, by means of $\vec{B}_{\rm eff}=-\partial\mathcal{H}/\partial\vec{m}$, one can write $\partial P_0/\partial\vec{m}=\beta\vec{B}_{\rm eff}P_0$, from which it follows that $\vec{m}\wedge\vec{B}_{\rm eff}P_0$ is divergenceless. On using these results, one sees by inspection that, in order to have the Boltzmann distribution as stationary solution of the Fokker-Planck equation (2.5), it is sufficient to set $\gamma(\lambda/m)=\beta/2\tau_{\rm N}$, from which one gets the following expression for the Néel time:

$$\tau_{\rm N}=\frac{1}{\lambda}\frac{m}{2\gamma k_{\rm B}T}. \tag{2.6}$$

Note that, since this result does not depend on the actual form of the Hamiltonian $\mathcal{H}$, it also holds for assemblies of interacting magnetic moments.

2. Comparison between the Landau-Lifshitz-Gilbert and Landau-Lifshitz stochastic models

Because the thermodynamic consistency of the approach determines $\tau_{\rm N}$ completely, we arrive at Eq. (2.6) both starting from Eqs. (2.1) and (2.4), so that *the Fokker-Planck equations associated with these stochastic models result to be identical*. Then, since $\tau_{\rm N}$ is related to the amplitude D of the fluctuating field by different expressions [Eq. (B8)], the only difference between these stochastic models lies in the relation among D, λ, and T. For the stochastic Landau-Lifshitz-Gilbert equation $\tau_{\rm N}^{-1}=2D\gamma^2(1+\lambda^2)$, whence

$$D_{\rm LLG}=\frac{\lambda}{1+\lambda^2}\frac{k_{\rm B}T}{\gamma m}, \tag{2.7}$$

whereas for the stochastic Landau-Lifshitz equation $\tau_{\rm N}^{-1}=2D\gamma^2$, so that

$$D_{\rm LL}=\lambda\frac{k_{\rm B}T}{\gamma m}. \tag{2.8}$$

These Einstein-type relations between the amplitude of the thermal-agitation field and the temperature, via the damping coefficient, ensure that the proper thermal-equilibrium properties are obtained from the stochastic Landau-Lifshitz (-Gilbert) equation. Thus, although the stochastic trajectories for a given realization of the fluctuating field $\vec{b}_{\rm fl}(t)$ are, in principle, different for each stochastic model, the average dynamical properties (which are determined by the Fokker-Planck equation) result to be identical in both approaches.

In the following sections we shall integrate the stochastic Landau-Lifshitz-Gilbert equation (2.1) numerically. Nevertheless, the above considerations ensure that, if we integrate the stochastic Landau-Lifshitz equation (2.4) instead, we shall obtain the same results for the *averaged* quantities.

3. Itô case

It is to be noted that the relations (2.7) and (2.8) [or equivalently Eq. (2.6)], being derived from Brown's Fokker-Planck equation (2.5), *pertain to the Stratonovich stochastic calculus*. Let us briefly examine this point. In order to construct the corresponding Fokker-Planck equation by using the Itô calculus, one simply omits the noise-induced drift when deriving the Fokker-Planck equation; this leads to an additional term $\tau_{\rm N}^{-1}\vec{m}$ into the square brackets of Eq. (2.5). Therefore, on using $\partial P_0/\partial t=0$ and Eq. (2.6) for $\tau_{\rm N}$, such an Itô Fokker-Planck equation yields for $P=P_0$

$$0=\frac{\partial}{\partial\vec{m}}\cdot(\vec{m}P_0)=(3+\beta\vec{m}\cdot\vec{B}_{\rm eff})P_0 \quad \text{(Itô case)},$$

which is not necessarily satisfied by a general form of the Boltzmann distribution $P_0(\vec{m})$ (that is, by a general form of the Hamiltonian). The simplest example is that of the dynamics in the absence of potential. Then $\vec{B}_{\rm eff}=0$ and the equilibrium distribution—$P_0(\vec{m})$ uniform—is not a solution of the Itô case of the Fokker-Planck equation. *Therefore, the stochastic Landau-Lifshitz (-Gilbert) equation, when interpreted in the Itô sense, does not yield the correct thermal-equilibrium properties.*

C. Equations for the averages

Let us finally consider the dynamical equations for the averages of the magnetic moment with respect to the nonequilibrium probability distribution $P(\vec{m},t)$. (Because these equations involve averaged quantities, they will be identical for both the stochastic Landau-Lifshitz-Gilbert and Landau-Lifshitz equations.)

The equation for the first moment $\langle m_i\rangle(t)=\int_{|\vec{m}|=m}d^3\vec{m}P(\vec{m},t)m_i$ reads

$$\frac{d}{dt}\langle\vec{m}\rangle=\gamma\langle\vec{m}\wedge\vec{B}_{\rm eff}\rangle-\gamma\frac{\lambda}{m}\langle\vec{m}\wedge(\vec{m}\wedge\vec{B}_{\rm eff})\rangle-\frac{1}{\tau_{\rm N}}\langle\vec{m}\rangle, \tag{2.9}$$

where the term $-\langle\vec{m}\rangle/\tau_{\rm N}$ is analogous to the relaxation term in a Bloch-type equation.[21] For the second-order moments $\langle m_i m_j\rangle(t)$ one finds

$$\frac{d}{dt}\langle m_i m_j\rangle=-\frac{3}{2\tau_{\rm N}}(\langle m_i m_j\rangle-\tfrac{1}{3}m^2\delta_{ij})+\gamma\langle m_i(\vec{m}\wedge\vec{B}_{\rm eff})_j\rangle$$
$$-\gamma\frac{\lambda}{m}\langle m_i[\vec{m}\wedge(\vec{m}\wedge\vec{B}_{\rm eff})]_j\rangle+i\leftrightarrow j, \tag{2.10}$$

where $i\leftrightarrow j$ stands for the interchange in the entire previous expression of the subscripts i and j.

Equations (2.9) and (2.10) show that, for a general form of the Hamiltonian, no closed equation exists for the time evolution of the averages of the magnetic moment. For instance, even if $\vec{B}_{\rm eff}$ does not depend on $\vec{m}$, the Landau-Lifshitz-type relaxation term introduces $\langle m_i m_j\rangle(t)$ in Eq. (2.9) for $\langle m_i\rangle(t)$. Therefore, an additional differential equation for $\langle m_i m_j\rangle(t)$ is required [i.e., Eq. (2.10)], however that equation involves $\langle m_i m_j m_k\rangle(t)$, and so on. *The absence of such a closed dynamical equation is a major source of mathematical difficulties in the theoretical study of the dynamical properties of classical spins*.

Free-diffusion case. A situation where the equations for the averages are not coupled and can in addition be explicitly solved, is that where the Hamiltonian is independent of $\vec{m}$ ($\vec{B}_{\rm eff}=0$). Note that, because $\tau_{\rm N}^{-1}\propto k_{\rm B}T$ [Eq. (2.6)], this apparently academic case can be a reasonable approximation for sufficiently high temperatures, where the terms multiplied by $\tau_{\rm N}^{-1}$ in Eqs. (2.9) and (2.10) dominate the remaining ones. The solutions of these equations for $\vec{B}_{\rm eff}=0$ are

$$\langle m_i\rangle(t)=\langle m_i\rangle(t_0)e^{-(t-t_0)/\tau_{\rm N}},$$

$$\langle m_i m_j\rangle(t)=\tfrac{1}{3}m^2\delta_{ij}+[\langle m_i m_j\rangle(t_0)-\tfrac{1}{3}m^2\delta_{ij}]e^{-3(t-t_0)/\tau_{\rm N}},$$

which justify calling the characteristic time constant $\tau_{\rm N}$ the *free-diffusion* time. For $(t-t_0)\gg\tau_{\rm N}$, one finds $\langle m_i\rangle(t)\to 0$ and $\langle m_i m_j\rangle(t)\to\frac{1}{3}m^2\delta_{ij}$, expressing that the orientations of $\vec{m}$ become distributed at random for long times, as it should for a diffusion in a constant orientational potential (or at very high temperatures). Note finally that these natural results are not obtained when one interprets the stochastic Landau-Lifshitz (-Gilbert) equation *à la* Itô.

III. TRAJECTORIES OF INDIVIDUAL MAGNETIC MOMENTS

In this section we shall study the $T\neq 0$ (stochastic) dynamics of *individual* magnetic moments. In order to provide the necessary background to undertake this study, in Appendix A we analyze solutions of the *deterministic* ($T\simeq 0$) Landau-Lifshitz equation. Here, we shall integrate the *stochastic* Landau-Lifshitz-Gilbert equation numerically in the context of the Stratonovich calculus, by means of the stochastic generalization of the Heun scheme. This scheme [a sort of second-order Runge-Kutta algorithm; see Eq. (C6)] and some details of its implementation are discussed in Appendix C.

A. System studied

Hereafter, the magnetic anisotropy of $\vec{m}$ will be assumed to have the simplest axial symmetry. Then, if $\vec{m}$ is subjected to an external constant (bias) field, $\vec{B}$, and a low probing field, $\Delta\vec{B}(t)$ [e.g., $\Delta\vec{B}(t)=\Delta\vec{B}_0\cos(\omega t)$], its Hamiltonian reads

$$\mathcal{H}(\vec{m},t)=-\vec{m}\cdot[\vec{B}+\Delta\vec{B}(t)]-\frac{Kv}{m^2}(\vec{m}\cdot\hat{n})^2, \tag{3.1}$$

where $\hat{n}$ is a unit vector along the symmetry axis and Kv is the anisotropy-energy barrier (we shall mainly consider anisotropy of easy-axis type, $K>0$). In terms of $B_K=2Kv/m$, the effective field [Eq. (2.2)] associated with the above $\mathcal{H}(\vec{m},t)$ can be written as

$$\vec{B}_{\rm eff}=[\vec{B}+\Delta\vec{B}(t)]+(B_K/m)(\vec{m}\cdot\hat{n})\hat{n}. \tag{3.2}$$

Accordingly, the quantity $|B_K|$ is the magnitude of the maximum *anisotropy field* $\vec{B}_{\rm a}=(B_K/m)(\vec{m}\cdot\hat{n})\hat{n}$, which occurs when $\vec{m}=\pm m\hat{n}$. Note that the anisotropy field decreases as $\vec{m}$ approaches the equatorial region ($\vec{m}\perp\hat{n}$), where it vanishes. On the other hand, in a longitudinal bias field ($\vec{B}\|\hat{n}$), $\mathcal{H}(\vec{m})$ has two minima at $\vec{m}=\pm m\,\hat{n}$, if $B<B_K$ (with a potential barrier between them of height $\Delta U=Kv$ for $B=0$), whereas the upper (shallower) potential minimum disappears for $B\geq B_K$.

Let us finally introduce some dimensionless quantities. B_K provides a suitable reference magnetic-field scale that yields the dimensionless fields

$$\vec{h}=\frac{\vec{B}}{B_K},\quad \vec{h}_{\rm eff}=\frac{\vec{B}_{\rm eff}}{B_K},\quad \vec{h}_{\rm fl}(t)=\frac{\vec{b}_{\rm fl}(t)}{B_K}. \tag{3.3}$$

A suitable time scale is provided by $\tau_K=(\lambda\gamma B_K)^{-1}$, which is the inverse of the deterministic ($T\simeq 0$) decay rate of the *angle* between $\vec{m}$ and $\hat{n}$ close to the bottom of the anisotropy-potential wells at $\vec{B}=0$, as obtained from the deterministic Landau-Lifshitz equation (see Appendix A). Thus, one has the dimensionless time

$$\underline{t}=\frac{t}{\tau_K},\quad \frac{1}{\tau_K}=\lambda\gamma B_K. \tag{3.4}$$

Note that in terms of τ_K, the Néel time (2.6) merely reads $\tau_{\rm N}=\sigma\tau_K$, where $\sigma=Kv/k_{\rm B}T$ is the dimensionless anisotropy-barrier height parameter.

B. The overbarrier rotation process

Figure 1 displays the projection of the trajectory of an individual magnetic moment with the simplest axially symmetric anisotropy potential onto selected planes. No magnetic field has been applied, so the graphs show the (in this sense) ''free'' dynamics.

The projection of $\vec{m}(t)$ onto a plane containing the anisotropy axis $\hat{n}$ (defining the $\hat{z}$ direction in Fig. 1), corresponds

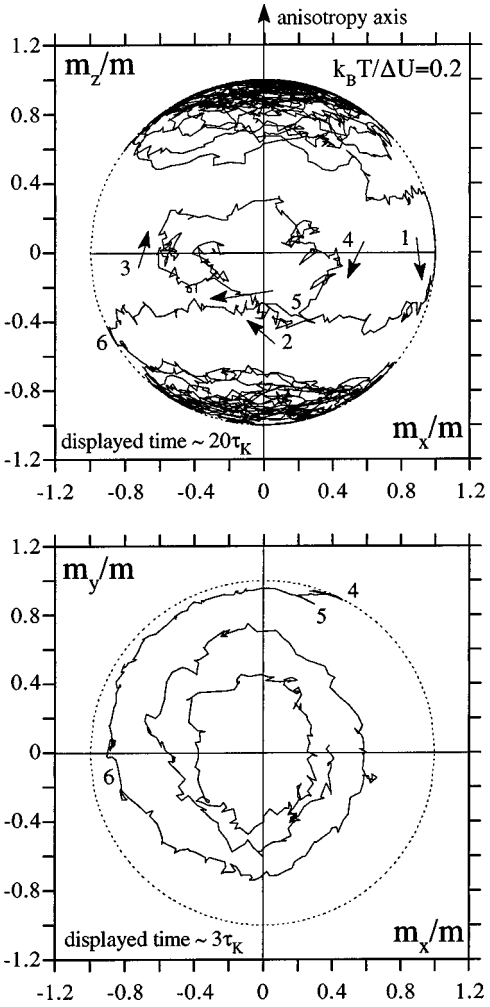

FIG. 1. Two-dimensional projections of the time evolution of the magnetic moment, as determined by numerical integration of the stochastic Landau-Lifshitz-Gilbert equation (2.1). The magnetic-anisotropy potential is $-\Delta U(m_z/m)^2$, no magnetic field has been applied, and the damping coefficient in the dynamical equation is $\lambda=0.1$. Upper panel: Projection of the trajectory onto a plane containing the anisotropy axis. Lower panel: Projection onto a plane perpendicular to the anisotropy axis of the first stages of the damped precession down to the $\vec{m}=-m\hat{z}$ potential minimum, after the last potential-barrier crossing. The small dashes demarcate the unit circle.

to a typical stochastic trajectory that starts close to one of the potential minima ($\vec{m}=m\hat{z}$) and, after some irregular rotations about it, reaches the potential-barrier (equatorial) region, where it wanders for a while, and eventually descends to the other potential minimum. Concerning the projection of this motion onto a plane perpendicular to the anisotropy axis, we have just shown the first stages, after the last potential-barrier crossing, of the damped precession of $\vec{m}$ about the anisotropy field, when spiraling down to the bottom of the $m_z<0$ potential well.

From these graphs, the role of the gyromagnetic terms in the stochastic dynamics of the magnetic moment is shown. Thus, the projection of $\vec{m}(t)$ onto the equatorial plane shows some of the irregular features of ordinary Brownian motion, although the rotary character is neatly exhibited. Concerning the projection of $\vec{m}(t)$ onto a plane containing the anisotropy axis, it is clearly seen that crossing the potential barrier does not entail an immediate descent to the other potential minimum, but the gyromagnetic terms plus an appropriate sequence of fluctuating fields can produce a rapid crossing back to the initial potential well.

For an ordinary, nongyromagnetic system, i.e., a mechanical system with inertia, this guarantees that, unless the system reaches the potential barrier with zero velocity, it will descend to the other potential well with a large probability. In addition, the forces, after the potential-barrier crossing, accelerate the system downward. However, in the gyromagnetic case the dynamics is ''noninertial'' (the equation of motion is of first order in the time). Besides, the anisotropy field $\vec{B}_a=(B_K/m)(\vec{m}\cdot\hat{n})\hat{n}$ indeed drives $\vec{m}$ down to the bottom of the potential well, but this is effected via a (damped) precession about the anisotropy axis. Moreover, the effective precession ''frequency'' of such motion $\omega_{\rm eff}=(\gamma B_K/m)(\vec{m}\cdot\hat{n})$ is initially rather low because the anisotropy field is low in the potential-barrier region ($\vec{m}\cdot\hat{n}\simeq 0$). Consequently, in the beginning of the spiraling down after a potential-barrier crossing, the magnetic moment rotates quite slowly (say, along a parallel of latitude) not far from the potential-barrier region, so that an appropriate sequence of fluctuations can drive $\vec{m}$ back to the initial potential well.

What is shown in Fig. 1 is precisely a multiple occurrence of this phenomenon; more than 10 potential-barrier crossings can be identified in the overall excursion between the two potential minima. On the other hand, the magnetic moment might also have eventually fallen into the original potential well. As will be shown below, none of these processes are infrequent. The physical acumen of Brown[15] is noteworthy since, on considering the gyromagnetic nature of the dynamics, he posed the possible occurrence of this kind of phenomena in his criticism of the calculation of Néel[1] of the relaxation time as the inverse of the rate of equatorial crossings of the magnetic moment.

C. The effect of the temperature

In order to assess the role of the temperature in the dynamics of the magnetic moment, we have displayed in Fig. 2 some typical time evolutions of the projection of $\vec{m}$ onto the anisotropy axis. It is seen that, at low temperatures (panel $k_BT/\Delta U=0.12$), the dynamics merely consist of the rotations of the magnetic moment close to the bottom of the potential wells (intra-potential-well relaxation modes), with the overbarrier relaxation mechanism being ''blocked.'' As T is increased, the magnetic moment can effect overbarrier rotations at the expense of the energy gained from the heat bath, and a number of them do occur during the displayed time interval (panels $k_BT/\Delta U=0.18$ and 0.28). Finally, at higher temperatures (panel $k_BT/\Delta U=0.4$), the magnetic moment effects a considerable number of overbarrier rotations during the observation time interval, exhibiting almost the thermal-equilibrium distribution of orientations.

The curves of Fig. 2 resemble those of the experiments of Wernsdorfer *et al.* on individual ferromagnetic nanoparticles (see Fig. 6 in Ref. 14). Furthermore, if the same trajectory is plotted with a larger sampling time interval, in order to

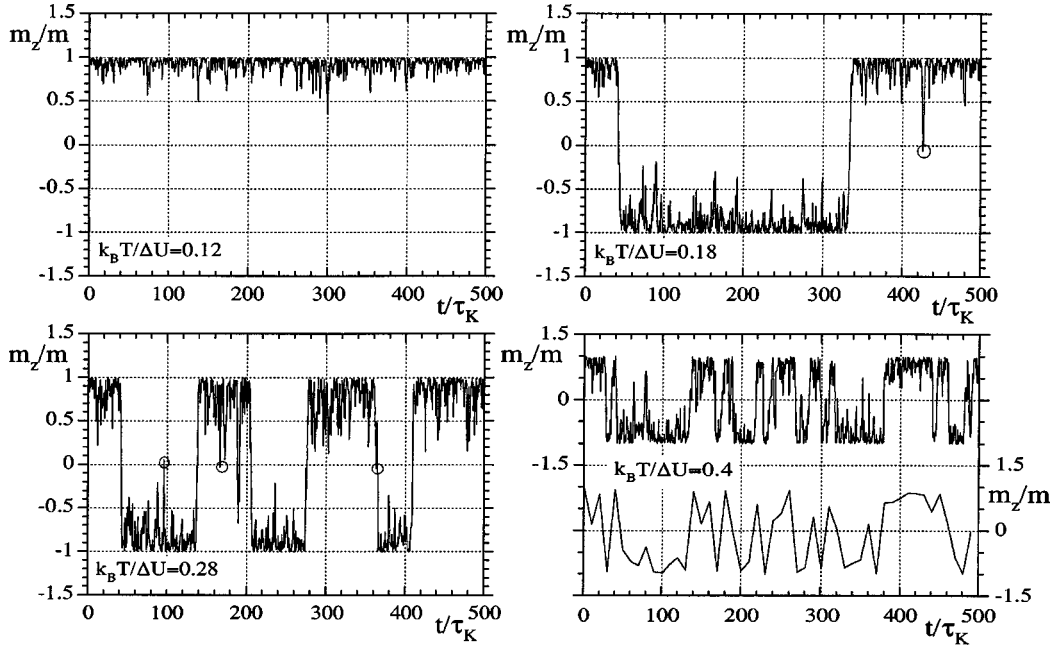

FIG. 2. Projection onto the anisotropy axis of $\vec{m}(t)$, as determined by numerical integration of the stochastic Landau-Lifshitz-Gilbert equation (2.1), for various temperatures. The magnetic-anisotropy energy is $-\Delta U(m_z/m)^2$, $\vec{B}=0$, and $\lambda=0.1$. The small circles mark potential-barrier crossings followed by a back rotation to the initial potential well. In the panel $k_BT/\Delta U=0.4$ such crossings have not been marked and the trajectory has also been plotted with a larger sampling time interval.

mimic the finite resolution time of a measuring device, the resemblance is more apparent, since the curves then have less and wider angles (see the panel $k_BT/\Delta U=0.4$). (Recall that the strong dependence of the appearance of the time evolution curves on the sampling period, is a typical feature of the stochastic dynamics.)

Note finally that in Fig. 2 a number of potential-barrier crossings followed by a rotation back to the original potential well can be identified (marked with small circles): one for $k_BT/\Delta U=0.18$; three for $k_BT/\Delta U=0.28$, the one occurring at $\sim 360t/\tau_K$ being a double crossing back; and about seven for $k_BT/\Delta U=0.4$ (not marked for the sake of clarity). It is also to be noted that an apparent single (or double) crossing back can be multiple instead. Indeed, when the about 10 potential-barrier crossings of Fig. 1 are represented as m_z vs t, they seem to be a mere double crossing back of the potential barrier.

D. Projection of $\vec{m}(t)$ onto the direction of a probing field

It is also illuminating to show the projection of the trajectories of individual spins onto the direction of a probing field $\Delta\vec{B}(t)=\Delta\vec{B}_0\cos(\omega t)$. Figure 3 shows such trajectories in the intermediate temperature range.

The projection onto the anisotropy axis direction $(\Delta\vec{B}_0\|\hat{n})$ exhibits, as in the corresponding case of Fig. 2, a well resolved bistability, and $\vec{m}$ ''jumps'' from one well to the other a number of times during a cycle of the probing field. Similar features are encountered when a longitudinal bias field is also applied, the main difference being that the lower potential well is less frequented by the magnetic moment. In contrast, the features of the stochastic trajectory obtained by projecting $\vec{m}(t)$ onto a direction perpendicular to the anisotropy axis $(\Delta\vec{B}_0\perp\hat{n})$ are markedly different (e.g., this projection corresponds to plotting the trajectory of the upper panel of Fig. 1 as m_x vs t). Here, the response is dominated by the fast $(\sim\tau_K)$ intra-potential-well relaxation modes, and the transverse projection is a highly irregular sequence of sharp peaks. Finally, the projection of $\vec{m}(t)$ onto $\Delta\vec{B}_0$ making an intermediate angle with the anisotropy axis ($\pi/4$ for the displayed curve), shows the magnetic bistability of the longitudinal projection, but the fast intra-potential-well motions are superimposed on it. This leads to a less well-resolved magnetic bistability.

Note finally that curves like those of Fig. 3 are the ones ''analyzed'' by the probing field in a dynamical ''measurement.'' Recall also that the application of the oscillating field hardly changes the overall features of the curves from the free evolution ones. This is naturally so, since one applies a low enough field in order to probe the intrinsic dynamics of the system.

IV. DYNAMIC RESPONSE OF THE ENSEMBLE OF SPINS

Keeping Figs. 2 and 3 in mind, we shall undertake the study of the dynamic response of an ensemble of classical magnetic moments. As a suitable probe of the intrinsic dynamics of the system, we shall compute the linear dynamic susceptibility $\chi(\omega)$ as a function of the temperature for various frequencies and orientations of an external probing field $\Delta\vec{B}(t)=\Delta\vec{B}_0\cos(\omega t)$. If one wishes to have a reference of the discussed time scales, one can assume, e.g., $B_K\sim 150$ mT and $\lambda\sim 0.01$–1, so that $\tau_K^{-1}\sim 0.1$–6×10^9 s^{-1} by Eq. (3.4) and the frequencies employed $(\omega\tau_K/2\pi\sim 10^{-3}$–$10^{-2})$ are then in the MHz range.

In the calculations presented in this section, ensembles of

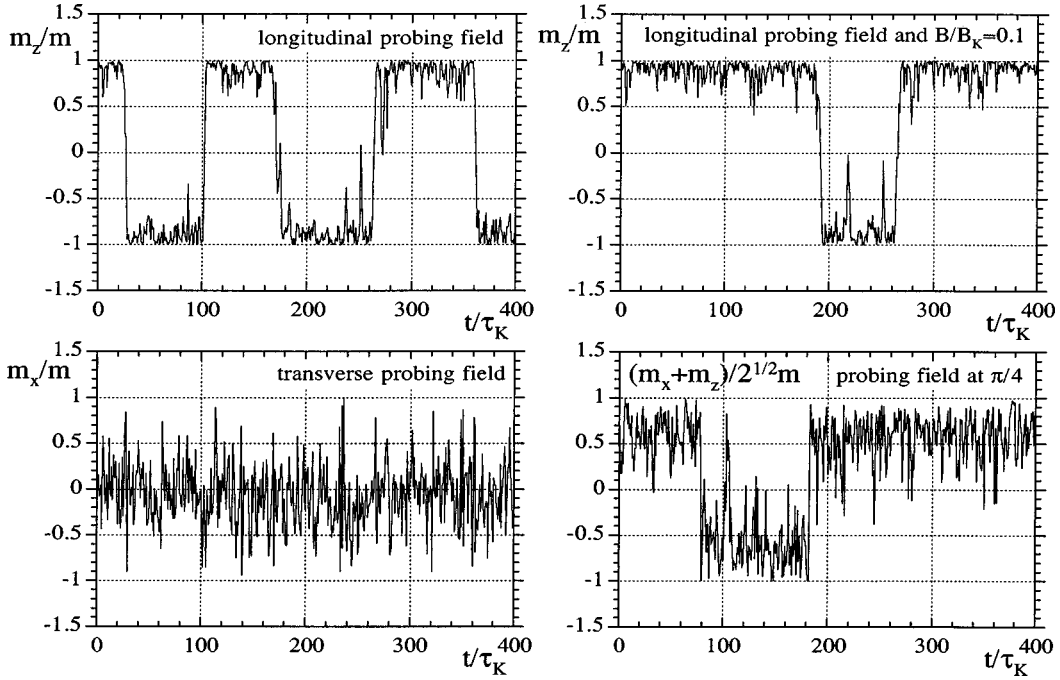

FIG. 3. Projection onto the direction of a probing field $\Delta\vec{B}(t)=\Delta\vec{B}_0\cos(\omega t)$ of $\vec{m}(t)$, as determined by numerical integration of the stochastic Landau-Lifshitz-Gilbert equation (2.1). The magnetic-anisotropy energy is $-\Delta U(m_z/m)^2$ and all the results are for $k_BT/\Delta U=0.2$ and $\lambda=0.1$. The displayed time interval corresponds to a complete cycle of the oscillating field ($\omega\tau_K/2\pi=0.0025$). In the longitudinal probing field case, results in the presence of a longitudinal bias field are also shown.

1000 magnetic moments have been employed. We integrate numerically the stochastic Landau-Lifshitz-Gilbert equation of each spin, by means of the stochastic Heun scheme (C6), and analyze the time evolution of the total magnetic moment of the ensemble; the results for the dynamic susceptibility have typically been averaged over 50–100 cycles of the oscillating field.

The damping coefficient λ, the magnetic-anisotropy potential barrier $\Delta U=Kv$, and the magnitude of the magnetic moment m have been assumed to be the same for each spin. (For noninteracting entities, the effects of a distribution of these parameters, as typically occurs in a nanoparticle ensemble, can be incorporated by an appropriate summation of the corresponding results.) In addition, as explained in Appendix C, in order to reduce the statistical error bars of the computed quantities, we apply at each temperature a sufficiently high probing field ($m\Delta B_0=0.3k_BT$) without leaving the *equilibrium* linear-response range.

Finally, in all the figures that follow, the linear susceptibilities are measured in units of $\mu_0 m/B_K=\mu_0 m^2/2Kv$ (the transverse equilibrium susceptibility per spin at zero temperature in the absence of a bias field). Furthermore, where they are not shown, the size of the statistical error bars of the numerical results is, at most, that of the plotted symbols.

A. Dynamic response in the absence of a bias field

We shall first study the response of the ensemble in the absence of a constant (bias) magnetic field.

1. Longitudinal response

Figure 4 displays the results for the longitudinal linear dynamic susceptibility vs the temperature for an ensemble of

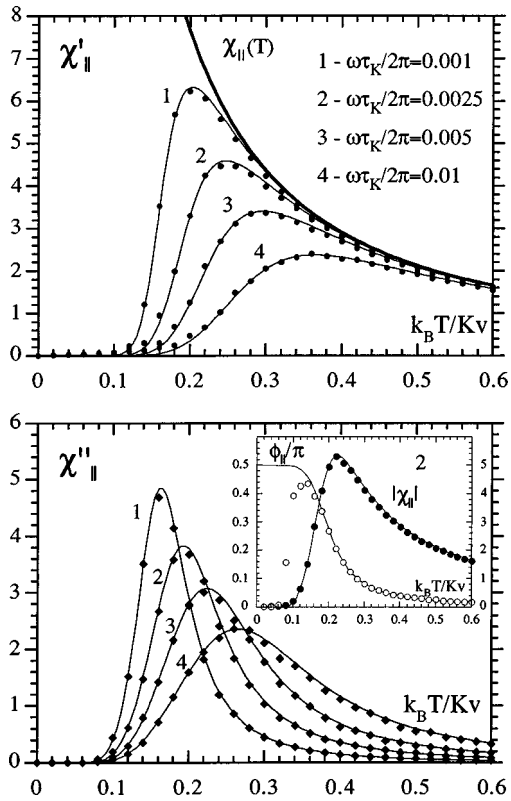

FIG. 4. Longitudinal linear dynamic susceptibility $\chi_\parallel$ vs T in the absence of a bias field. The symbols are for the numerically computed $\chi_\parallel(\omega,T)$ and the thin solid lines are Eq. (D10) with $\tau_\parallel$ defined as integral relaxation time [Eq. (D13)]. The thick solid line in the upper panel is the thermal-equilibrium susceptibility [Eq. (D4)]. Inset: Modulus and phase shift of $\chi_\parallel$ for $\omega\tau_K/2\pi=0.0025$.

magnetic moments with parallel anisotropy axes $[\Delta\vec{B}(t)\|\hat{n}]$. No bias field has been applied and a damping coefficient $\lambda = 0.1$ has been used. (Because of the axial symmetry considered, the effect of λ on the averaged quantities merely enters via the Néel time $\tau_N = \sigma\tau_K$, as can be shown from Brown's Fokker-Planck equation. Thus, since we measure the time and the frequencies in units of τ_K, the results presented for the *longitudinal* response must be independent of the λ used.)

At low temperatures the longitudinal relaxation time $\tau_\parallel$ obeys the condition $\tau_\parallel \gg 2\pi/\omega$ [$t_m(\omega) = 2\pi/\omega$ is the *dynamical* measurement time]. Consequently, over a large number of cycles of the probing field the probability of overbarrier rotations is almost zero; the response consists of the rotations of the magnetic moments close to the bottom of the potential wells (see the panel $k_BT/\Delta U = 0.12$ of Fig. 2), whose averaged (over the ensemble) projection onto the probing-field direction is small (but nonzero; see the enlargement of the low-T range in the inset of Fig. 8). Moreover, as these intra-potential-well relaxation modes are very fast ($\sim\tau_K$), this small response is in phase with the probing field {see the low-T part of the phase shift $\phi(\omega,T) = \arctan[\chi''(\omega,T)/\chi'(\omega,T)]$ in the inset of Fig. 4}.

As T is increased the magnetic moments can depart from the potential minima by means of the energy gained from the heat bath. Consequently, at an ω-dependent temperature ($k_BT/Kv \sim 0.1$–0.2 for the frequencies employed), which increases with increasing ω, a small probability of surmounting the magnetic-anisotropy potential barrier during a number of cycles of the probing field, emerges (this corresponds to the panel $k_BT/\Delta U = 0.18$ of Fig. 2). Accordingly, the averaged response starts to increase steeply with T. However, as this thermally activated response mechanism via overbarrier rotations is not efficient enough at these temperatures, the signal exhibits a considerable lag behind the probing field (see the inset of Fig. 4). This is also reflected by the occurrence of a sizable out-of-phase component of the response, $\chi''_\parallel(T)$ (in fact the response is mainly ''out of phase'').

At higher temperatures, the mechanism of overbarrier rotations becomes increasingly efficient (panel $k_BT/\Delta U = 0.28$ of Fig. 2). Consequently, after exhibiting a maximum, the phase shift starts to *decrease* whereas the magnitude of the response still *increases* steeply with T (see the inset of Fig. 4). However, if the temperature is further increased, the very thermal agitation, which up to these temperatures was responsible for the increase in the magnitude of the response, reaches a value that (i) efficiently produces overbarrier rotations, allowing the magnetic moments to approximately redistribute according to the instantaneous probing field, but, simultaneously, (ii) disturbs sizably the alignment of the magnetic moments in the probing-field direction. Consequently, at a T above that of the phase maximum ($k_BT/Kv \sim 0.2$–0.3 for the frequencies considered), the magnitude of the response has a maximum and starts to decrease with increasing T. The frequency-dependent temperature at which this maximum occurs is usually called the *blocking* temperature.

Finally, at still higher temperatures ($k_BT/Kv \gtrsim 0.3$–0.5 for the frequencies considered) the inequality $\tau_\parallel \ll 2\pi/\omega$ holds. Thus, in comparison to $\tau_\parallel^{-1}$, the rate of change of the probing field is quasistationary. Consequently, the magnetic moments quickly redistribute according to the conditions set by the instantaneous probing field, almost being in the thermal-equilibrium state associated with it (panel $k_BT/\Delta U = 0.4$ of Fig. 2). Then, the $\chi'_\parallel(T)$ curves corresponding to different frequencies sequentially superimpose on the equilibrium linear susceptibility $\chi_\parallel(T)$ and, correspondingly, $\chi''_\parallel(T)$ approaches zero.

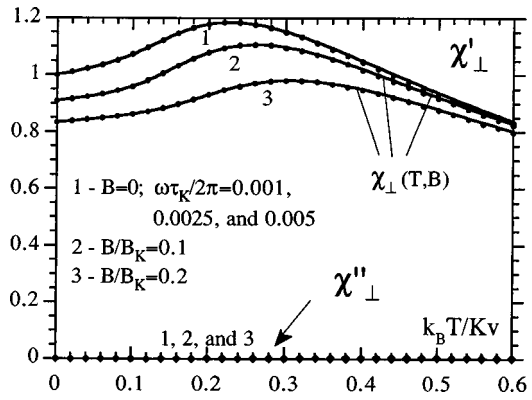

FIG. 5. Transverse linear dynamic susceptibility $\chi_\perp$ vs T for the frequencies $\omega\tau_K/2\pi = 0.001$, 0.0025, and 0.005. The damping coefficient is $\lambda = 0.1$. Results in the unbiased ($B = 0$) case and in the presence of the longitudinal bias fields $B/B_K = 0.1$ and 0.2 (for $\omega\tau_K/2\pi = 0.005$ only) are shown. The thick solid lines are the equilibrium susceptibilities [Eq. (D4)]. $\chi'_\perp$ (circles) and $\chi''_\perp$ (rhombi) have intentionally been plotted with the same scale to show the relative smallness of the latter.

The appearance of a frequency-dependent maximum in the response of a noisy nonlinear multistable system to a periodic stimulus, as a function of the noise intensity, is one of the features usually accompanying *stochastic resonance*. In this spin-dynamics case, the maximum in the magnitude of the dynamic response as a function of T, can be understood in terms of the quoted twofold role played by the temperature: (i) activating the dynamics of overbarrier rotations, allowing the spins to (statistically) follow the instantaneous field, but, (ii) provoking the thermal misalignment of the spins from the driving-field direction.

2. Transverse response

We shall now study the *transverse* dynamic response of an ensemble of magnetic moments with parallel anisotropy axes $[\Delta\vec{B}(t)\perp\hat{n}]$. Figure 5 displays $\chi_\perp(\omega)$ vs T for various frequencies of the probing field (curves labeled 1; results in the presence of a bias field to be discussed below are also shown).

For this transverse probing-field geometry, the mechanism of inter-potential-well rotations plays a minor dynamical role, since it mainly pertains to the components of the magnetic moments perpendicular to the probing field, whereas the response in the probing-field direction is the one recorded. The latter consists of intra-potential-well rotations, which are very fast ($\sim\tau_K$; see the panel $\Delta\vec{B}_0\perp\hat{n}$ of Fig. 3) as compared to $t_m(\omega) = 2\pi/\omega$. Consequently, the dynamic susceptibilities obtained are close to the equilibrium susceptibility in the whole temperature range. Indeed, the $\chi'_\perp(T)$ curves corresponding to different frequencies are very close

to one another (they visually coincide) and almost describe the equilibrium susceptibility $\chi_\perp(T)$ (thick solid line), while the out-of-phase component $\chi''_\perp(T)$ is small. In addition, $\chi''_\perp$ is not only small as compared to $\chi'_\perp$ but it is also much smaller than the out-of-phase longitudinal susceptibility $\chi''_\parallel$ (cf. Fig. 4). Nevertheless, $\chi''_\perp$ provides interesting information concerning the dynamics of $\vec{m}$, which will be discussed in Sec. IV C.

For the transverse response, the maximum of $\chi'_\perp$ vs T is due to the crossover from the free-rotator regime ($Kv \ll k_BT$) to the discrete-orientation regime ($Kv \gg k_BT$), induced by the bistable magnetic-anisotropy potential. At low temperatures the transverse probing field competes with the anisotropy energy in aligning the magnetic moments, which are concentrated close to the potential minima ($\vec{m} = \pm m\hat{n}$). Then, the increase of the thermal agitation allows $\vec{m}$ to (statistically) separate from the minima and the (transverse) response increases. However, as the temperature is further increased $\vec{m}$ becomes increasingly unfastened from the anisotropy and the transverse field competes mainly with the thermal agitation in aligning $\vec{m}$; the response then exhibits a maximum and decreases as T is further increased. Note that this is essentially a *thermal-equilibrium* effect, with a markedly different character from the *dynamical* maxima exhibited by the longitudinal susceptibility $\chi_\parallel(\omega,T)$.

3. Response for anisotropy axes distributed at random

Finally, owing to the linearity of the response, when a distribution in anisotropy-axis orientations occurs, $\chi(\omega)$ *in the absence of a bias field* is merely given by the weighted sum of the longitudinal and transverse dynamic susceptibilities, the weight factors being $\langle\cos^2\alpha\rangle$ and $\langle\sin^2\alpha\rangle$, respectively. (The angular brackets enclosing functions of α, which is the angle between the anisotropy axis and the probing field, or susceptibilities, stand for average over the anisotropy axis distribution of an ensemble with the same parameters λ, Kv, and m.)

The linear dynamic susceptibility for anisotropy axes distributed at random ($\langle\cos^2\alpha\rangle = \langle\sin^2\alpha\rangle/2 = 1/3$) is displayed in Fig. 6. The out-of-phase component, $\langle\chi''(\omega,T)\rangle_{\rm ran}$, is overwhelmingly dominated by the responses to the components of the probing field *along* the different anisotropy axes, and it is almost $\frac{1}{3}\chi''_\parallel(\omega,T)$ (cf. Fig. 4). On the other hand, the in-phase component, $\langle\chi'(\omega,T)\rangle_{\rm ran}$, is approximately $\frac{1}{3}\chi'_\parallel(\omega,T)$ plus a nonuniform upwards shift of magnitude $\frac{2}{3}\chi_\perp(T)$, where $\chi_\perp(T)$ is the equilibrium transverse susceptibility. This occurs in such a way that (i) at high temperatures, the Curie law $\mu_0 m^2/3k_BT$ [equilibrium $\langle\chi(T)\rangle_{\rm ran}|_{B=0}$; see, e.g., Refs. 22,23] is obeyed and (ii) at temperatures well below the blocking temperatures, the response consists mainly of the projection in the probing field direction of the rotations of the magnetic moments close to the bottom of the potential wells ($\frac{2}{3}\chi_\perp|_{T\simeq 0}$). Due to the short characteristic time of these intra-potential-well rotations ($\sim\tau_K$; see Fig. 3), this low-temperature response is nearly instantaneous and in phase with the probing field (see the inset of Fig. 6).

B. Dynamic response in a longitudinal bias field

We shall now study the effects of a constant magnetic field $\vec{B}$ applied along the common anisotropy axis direction of a spin ensemble with parallel anisotropy axes ($\vec{B}\|\hat{n}$).

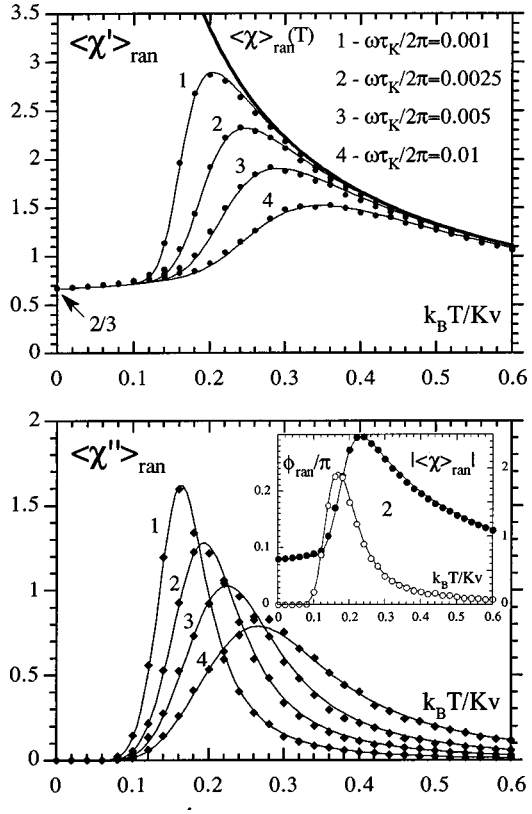

FIG. 6. Linear dynamic susceptibility vs T for anisotropy axes distributed at random, $B=0$, and $\lambda=0.1$. The symbols are for the numerically computed $\langle\chi(\omega,T)\rangle_{\rm ran}$ and the thin solid lines are Eq. (D10) with $\tau_\parallel$ defined as integral relaxation time [Eq. (D13)], and $\tau_\perp$ given by the modified effective eigenvalue result (D15). The thick solid line in the upper panel is the thermal-equilibrium susceptibility $\langle\chi(T)\rangle_{\rm ran}|_{B=0} = \mu_0 m^2/3k_BT$. Inset: Modulus and phase shift of $\langle\chi(\omega,T)\rangle_{\rm ran}$ for $\omega\tau_K/2\pi = 0.0025$.

1. Longitudinal response

Figure 7 displays the longitudinal $[\Delta\vec{B}(t)\|\hat{n}\|\vec{B}]$ linear dynamic susceptibility vs the temperature for various values of the bias field. The qualitative features of the susceptibility curves are similar to those encountered in the unbiased ($B=0$) case, and can be interpreted in terms of the same processes: (i) At low temperatures the response consists of the fast rotations of the magnetic moments close to the bottom of the potential wells, with the overbarrier relaxation mechanism being blocked. (ii) As T is increased the magnetic moments can depart from the potential minima, by means of the energy gained from the heat bath, and the response starts to increase steeply with T (with a sizable lag behind the probing field). (iii) If T is further increased the system reaches the regime dominated by inter-potential-well rotations, exhibiting dynamical maxima first in the phase shift and subsequently in the magnitude of the response. (iv) In the high-temperature range, the magnetic moments are almost in the thermal-equilibrium state associated with the instantaneous probing field and, hence, $\chi'_\parallel(T,B)$ tends to the equilibrium linear susceptibility while $\chi''_\parallel(T,B)$ approaches zero.

Thus, the dynamics is qualitatively similar to that of the unbiased case, the main difference being that the system now consists of bistable *nonsymmetrical* entities. The two potential wells, which do exist since the applied bias fields are

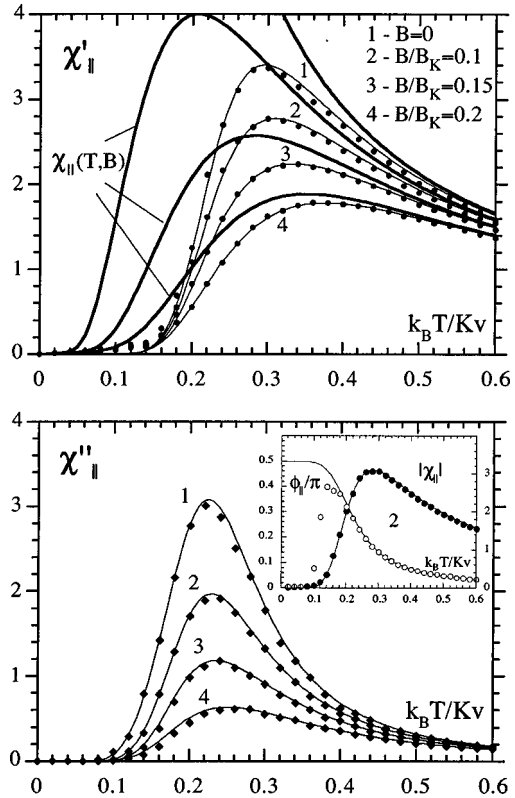

FIG. 7. Longitudinal linear dynamic susceptibility $\chi_{\parallel}$ vs T, for $\lambda=0.1$, $\omega\tau_K/2\pi=0.005$, and various values of the longitudinal bias field. The symbols are for the numerically computed $\chi_{\parallel}(\omega,T,B)$ and the thin solid lines are Eq. (D10) with $\tau_{\parallel}$ defined as integral relaxation time [Eq. (D13)]. The thick solid lines in the upper panel are the corresponding equilibrium susceptibilities [Eq. (D4)]. Inset: Modulus and phase shift of $\chi_{\parallel}(\omega,T,B)$ for $B/B_K=0.1$.

below the critical one $B=B_K$ where the upper (shallower) potential well disappears, now have different depths. Furthermore, the magnitude of the equilibrium response is smaller than that of the unbiased case, and decreases with increasing B, since the equilibrium $\chi_{\parallel}(T,B)$ is the slope of the magnetization vs field curve at B, instead of the initial slope of the unbiased case.

We remark in passing that the simple idea that the application of a constant magnetic field reduces the potential barriers, so that the relaxation rate increases and the blocking temperatures shift to lower temperatures, should be viewed with caution. The location of the maximum of the dynamic response indeed depends on the potential-barrier heights, but also on the form of the equilibrium response, which is markedly different from that of the unbiased case. (In a bias field the equilibrium response exhibits a maximum as a function of T and then decreases to zero as T is lowered, since $\chi_{\parallel}(T,B)$ is the slope of the longitudinal magnetization curve at B and, for a fixed finite B, the magnetization saturates at low T.) Indeed, for the frequencies and bias fields considered, the location of the maxima of $\chi''_{\parallel}(T)$ is not very sensitive to the bias field, while those of $\chi'_{\parallel}(T)$ shift slightly to higher temperatures as B increases.

2. Transverse response

We shall finally consider the *transverse* dynamic response in the presence of a *longitudinal* bias field $[\Delta\vec{B}(t)\perp\hat{n}\|\vec{B}]$. Figure 5 also displays $\chi_{\perp}(\omega,T,B)$ vs T for $B/B_K=0.1$ and 0.2 (curves labeled 2 and 3, respectively) and $\omega\tau_K/2\pi=0.005$. The qualitative features of the susceptibility curves are similar to those encountered in the unbiased case: (i) the mechanism of inter-potential-well rotations plays a minor dynamical role, with the response being dominated by the fast intra-potential-well rotations, (ii) the $\chi'_{\perp}(T,B)$ curves obtained are rather close to the corresponding equilibrium susceptibilities (thick solid lines), and (iii) $\chi''_{\perp}(T,B)$ is small as compared to both $\chi'_{\perp}(T,B)$ and $\chi''_{\parallel}(T,B)$.

C. Comparison of the numerical results with different analytical expressions

We shall finally compare the linear dynamic susceptibility, obtained by numerical integration of the stochastic Landau-Lifshitz-Gilbert equation, with the heuristic models discussed in Appendix D and rigorous expressions. In this comparison *no adjustable parameter* will be employed.

We shall sometimes use the word *exact* when referring to the numerical results. Along with the considerations of Appendix C about the feasible diminishing of the statistical error bars of the computed quantities by averaging over a sufficiently large number of trajectories, we also implicitly mean that the numerical results are *exact* in the context of the Brown-Kubo-Hashitsume stochastic model.

1. Longitudinal response

Figure 8 shows the computed $\chi_{\parallel}(\omega)$ in the unbiased case and in the bias field $B/B_K=0.1$. The predictions of the discrete-orientation [Eq. (D12)]; Gittleman, Abeles, and Bozowski [Eq. (D10) with the approximate Eq. (D7)]; and Shliomis and Stepanov [Eq. (D10)] heuristic models for the dynamic susceptibility are also shown. The longitudinal relaxation time $\tau_{\parallel}$ defined as the *integral relaxation time* $\tau_{\mathrm{int},\parallel}$ [Eq. (D13)] has been incorporated in the three equations.

It is apparent that Eq. (D12) fails to describe the numerical results; neither is the equilibrium (high-temperature) susceptibility properly described. Indeed, the overall failure of this expression could mainly be attributed to the rough approximation used for its equilibrium part [Eq. (D9)]. The probability that $\vec{m}$ makes a finite angle with the anisotropy axis is completely neglected in such a discrete-orientation equation.

Concerning the Gittleman, Abeles, and Bozowski equation, it is more suitable than the previous one, especially for the matching of $\chi''_{\parallel}(T,B)$, although it fails to describe $\chi'_{\parallel}(T,B)$. Again, not even the equilibrium susceptibility is correctly described; the high-barrier approximation for $\chi_{\parallel}(T,B)$ occurring in this model [Eq. (D7)], although better than the discrete-orientation approximation, is still not accurate enough at the relevant temperatures. Furthermore, for bias fields $B/B_K\gtrsim 0.15$, the divergence of this model from the exact results becomes dramatic (curves not shown).

In contrast, Eq. (D10) approximates the numerical results reasonably. Recall that the exact expression for $\chi_{\parallel}(\omega)$ comprises an infinite number of Debye-type relaxation mechanisms, namely,

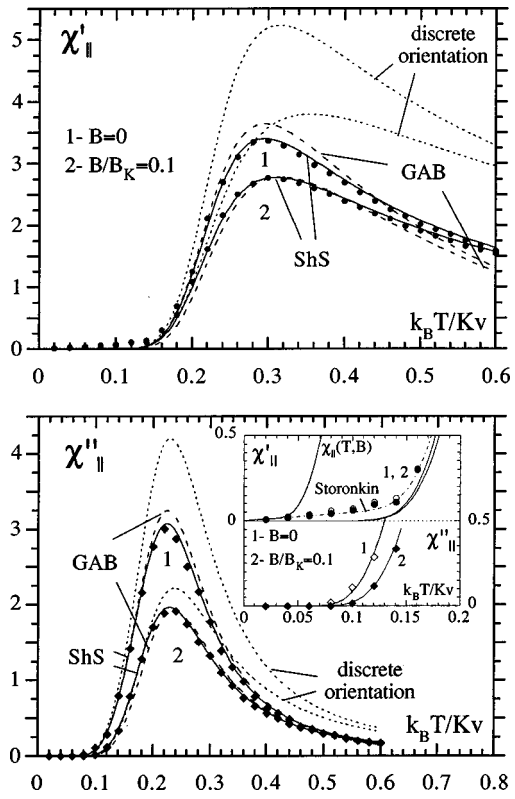

FIG. 8. $\chi_\parallel$ vs T for $B=0$ and $B/B_K=0.1$ with $\omega\tau_K/2\pi=0.005$ (symbols). The short-dashed line is for Eq. (D12), the medium-dashed line for Eq. (D10) with the approximate Eq. (D7), and the solid lines for Eq. (D10). $\tau_\parallel$ defined as integral relaxation time [Eq. (D13)] has been incorporated in the three heuristic models. Inset: Enlargement of the low-temperature part of $\chi_\parallel$ vs T showing the effect of the intra-potential-well relaxation modes. The thick solid line is the equilibrium susceptibility for $B/B_K=0.1$, the thin solid lines are again for Eq. (D10), and the dashed-dotted lines for the asymptotic result (4.2) by Storonkin (for $B=0$ only). For $\chi_\parallel''$, Eqs. (D10) and (4.2) visually coincide.

$$\chi_\parallel(\omega,T,B)=\chi_\parallel(T,B)\sum_{k=1}^{\infty}\frac{a_k(T,B)}{1+i\omega/\Lambda_k(T,B)}, \qquad (4.1)$$

where a_k ($\Sigma_{k\geqslant 1}a_k=1$) is the amplitude corresponding to the eigenvalue Λ_k ($0<\Lambda_1\leqslant\Lambda_2\cdots$) of the Sturm-Liouville equation associated with the Fokker-Planck equation. The first nonvanishing eigenvalue Λ_1 is associated with the inter-potential-well dynamics, whereas the higher-order eigenvalues Λ_k, $k\geqslant 2$ are related to the intra-potential-well relaxation modes. Therefore, the mentioned agreement could be expected in the unbiased case since, as it was shown numerically by Coffey *et al.*:[9] (i) $a_1(B=0)\gg a_k(B=0),\forall k\geqslant 2$ and (ii) $\Lambda_1^{-1}(B=0)\simeq\tau_{\mathrm{int},\parallel}(B=0)$. Indeed, in Ref. 24 it was shown that an expression equivalent to the longitudinal component of Eq. (D10), together with the interpolation formula of Cregg, Crothers, and Wickstead[25] for Λ_1^{-1}, describes well the longitudinal dynamic polarizability of the congeneric nematic liquid crystal with Meier-Saupe potential in the absence of a bias field. (The *longitudinal* relaxation in this system is mathematically identical with that of classical magnetic moments.) In addition, although in a constant longitudinal field the higher-order modes can make a substantial contribution *in the low-temperature* ($\sigma=Kv/k_BT\gg 1$) *region* (Λ_1^{-1} can then largely deviate from $\tau_{\mathrm{int},\parallel}$ and $a_1\gg a_k$ no longer holds; see Ref. 11), for the frequencies employed here, the relevant dynamical phenomena occur in the range $\sigma\sim 3-5$, so that, for the bias fields applied, Eq. (D10) describes the exact results reasonably.

However, one could expect, even for $B=0$, a significant contribution of the intra-potential-well relaxation modes to the longitudinal response when the overbarrier dynamics is *blocked* at low T ($\omega/\Lambda_1\gg 1$). Indeed, when scrutinizing Figs. 4 and 7, one sees that Eq. (D10) predicts, both for $B=0$ and $B\neq 0$, a smaller $\chi_\parallel'$, when departing from zero at temperatures well below the blocking temperatures, than the exact $\chi_\parallel'$. In addition, because the intra-potential-well relaxation modes are very fast ($\sim\tau_K$), their contribution to the out-of-phase susceptibility is smaller than their contribution to $\chi_\parallel'$, so that $\chi_\parallel''$ is still described reasonably by the Debye-type term associated with the inter-potential-well dynamics ($\chi_\parallel''\simeq\chi_\parallel(\omega/\Lambda_1)/[1+(\omega/\Lambda_1)^2]$).

These considerations are substantiated by comparing the numerical results with the asymptotic ($\sigma\gg 1$) expression for the longitudinal dynamic susceptibility of the nematic liquid crystal derived by Storonkin,[26] namely,

$$\chi_\parallel\simeq\frac{\mu_0 m^2}{k_BT}\left[\left(1-\frac{1}{\sigma}-\frac{3}{4\sigma^2}\right)\frac{1}{1+i\omega/\Lambda_1}+\frac{1}{8\sigma^2}\left(\frac{1}{1+i\omega/\Lambda_3}+\frac{1}{1+i\omega/\Lambda_5}\right)\right], \qquad (4.2)$$

where

$$\Lambda_1^{-1}\simeq\tau_N\frac{\sqrt{\pi}}{2}\sigma^{-3/2}\exp(\sigma)\left(1+\frac{1}{\sigma}+\frac{7}{4\sigma^2}\right), \qquad (4.3)$$

$$\Lambda_3^{-1}\simeq\Lambda_5^{-1}\simeq\frac{1}{2}\frac{\tau_N}{\sigma}\left(1+\frac{5}{2\sigma}+\frac{41}{4\sigma^2}\right). \qquad (4.4)$$

[Note that $(\mu_0 m^2/k_BT)(1-1/\sigma-3/4\sigma^2)\simeq\chi_\parallel(T)+\mathcal{O}(1/\sigma^2)$, while the result for Λ_1^{-1} agrees with that by Brown;[27] see also Ref. 9.] In the inset of Fig. 8 it is shown that Eq. (4.2) remarkably describes the $B=0$ numerical results at low temperatures. Because $\Lambda_{3,5}\sim\tau_N/\sigma=\tau_K$ and $\omega\tau_K\ll 1$ for the frequencies considered, it follows that $1/(1+i\omega/\Lambda_{3,5})\simeq 1-i\omega/\Lambda_{3,5}$. Therefore, since $(\mu_0 m^2/k_BT)\times(1/8\sigma^2)\propto k_BT$, Storonkin formula (4.2) yields the low-temperature linear increase of $\chi_\parallel'$ with T due to the intra-potential-well relaxation modes, whereas their contribution to $\chi_\parallel''$ is smaller by a factor $\omega/\Lambda_{3,5}\sim\omega\tau_K$.

This takes a dramatic reflection in the phase shifts. As any expression of the form $\chi(\omega)=\chi/(1+i\omega\tau)$ (Debye type), the *longitudinal* component of Eq. (D10) yields a phase shift $\phi_{\mathrm{ShS},\parallel}=\arctan(\omega\tau_\parallel)$, which increases monotonically with decreasing T (corresponding to the emergence of a sizable $\chi_\parallel''$) and, eventually, reaches $\pi/2$ (see the insets of Figs. 4 and 7), since at low temperatures $\omega\tau_\parallel\gg 1$. However, since the fast intra-potential-well relaxation modes yield an almost instantaneous contribution to the response, $\chi_\parallel'$ decreases with T less steeply than $\chi_\parallel/[1+(\omega/\Lambda_1)^2]$ at low temperatures,

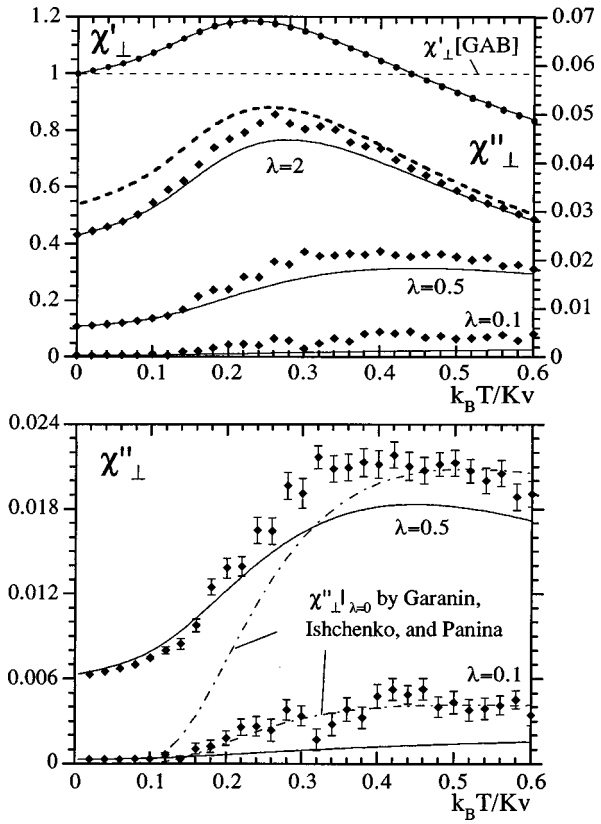

FIG. 9. Upper panel: $\chi_\perp$ vs T for $B=0$, $\omega\tau_K/2\pi=0.005$, and various values of the damping coefficient λ. The circles are for $\chi'_\perp$, and the rhombi for $\chi''_\perp$. The medium dashed line corresponds to the constant $\chi'_\perp$ given by Eq. (D11) and the solid lines to Eq. (D10) with $\tau_\perp$ given by Eq. (D15). The thick dashed curve is $\chi''_\perp(\omega,T)$ with $\tau_\perp$ given by the $\lambda\gg1$ result (D14). Lower panel: Detail of $\chi''_\perp(\omega,T)$ in the intermediate-to-weak damping regime together with the exact zero-damping formula (4.5) of Garanin, Ishchenko, and Panina (dashed-dotted lines).

whereas $\chi''_\parallel$ is still approximately given by $\chi_\parallel(\omega/\Lambda_1)/[1+(\omega/\Lambda_1)^2]$. Consequently, the actual phase shift (insets of Figs. 4 and 7), also increases monotonically with decreasing T but, at a temperature close to that of the peak of $\chi''_\parallel(T)$, $\phi_\parallel(T)$ exhibits a maximum and then decreases to zero as T is further lowered, since at low T, due to the fast intra-potential-well relaxation modes, the response is again ''in phase'' with the probing field. This behavior of the phase shift, which is in agreement with the results of Ref. 10, is qualitatively similar to that encountered in one-dimensional bistable systems,[28] and ascribed to the crossover from the high-noise regime, dominated by inter-potential-well jumps, to the low-noise regime, dominated by the fast intra-potential-well motions.

2. Transverse response

Figure 9 displays the corresponding comparison for $\chi_\perp(\omega)$ in the unbiased case for various values of the damping coefficient. For the transverse relaxation time $\tau_\perp$ we have used Eq. (D15), which has been derived (Appendix D) from the low-frequency expansion of the equation for $\chi_\perp(\omega)$ of Raĭkher and Shliomis.[29,30] (In the frequency range below the ferromagnetic resonance range the $\chi_\perp(\omega)$ of these authors is indistinguishable from the low-ω expansion used here.)

For the transverse probing-field geometry, the discrete-orientation formula (D12) predicts obviously an identically zero response, while the Gittleman, Abeles, and Bozowski formula yields a constant $\chi'_\perp(T)$ and a zero $\chi''_\perp(T)$. In contrast, the exact $\chi'_\perp(T)$ is described well by Eq. (D10), although, because $\omega\tau_\perp\ll1$ holds in the considered frequency range, $\chi'_\perp(T)$ almost coincides with the equilibrium susceptibility $\chi_\perp(T)$. Concerning $\chi''_\perp(T)$, Eq. (D10) with the expression (D15) for $\tau_\perp$ only matches the out-of-phase response in the low-temperature range ($Kv/k_BT\gtrsim7$) for the smallest damping coefficient used ($\lambda=0.1$). Nevertheless, Fig. 9 shows that, as the damping coefficient is enlarged, the matching between the numerical results and the simple Eq. (D10) improves when one uses the $\tau_\perp$ proposed [Eq. (D15)]. This constitutes an advance over the usual approach, where one uses the $\tau_\perp$ derived by the effective-eigenvalue method [Eq. (D14)], which yields the thick dashed curve of Fig. 9 *irrespective of* λ.

The above comparison is in agreement with that made by Kalmykov and Coffey[31] of their numerical results, obtained by continued-fraction techniques, with the complete (but approximate) expression for $\chi_\perp(\omega,T)$ of Raĭkher and Shliomis.[29,30] The failure of this expression for weak damping was explained in terms of the effects of the gyromagnetic terms of the dynamical equation. When these terms dominate ($\lambda\ll1$), due to the occurrence of a spread of the precession frequencies of $\vec{m}$ in the anisotropy field at intermediate temperatures [these frequencies are $\propto\gamma B_K(\vec{m}\cdot\hat{n})$], the response is not well described by a simple relaxation mechanism. Thus, only at low temperatures, where the magnetic moments are concentrated close to the bottom of the potential wells (so the spread in precession frequencies is reduced), the exact results are well described by the $\chi_\perp(\omega,T)$ of Raĭkher and Shliomis [or equivalently by Eq. (D10) with the expression (D15) for $\tau_\perp$].

The effects of the spread of the precession frequencies of $\vec{m}$ in the anisotropy field had already been investigated by Garanin, Ishchenko, and Panina.[21] They derived from the Fokker-Planck equation the *exact* expression for $\chi''_\perp(\omega,T,B)$ in the $\lambda\to0$ limit, which fully accounts for the effects of this phenomenon. Their formula can be written as

$$\chi''_\perp|_{\lambda=0}=\frac{\mu_0 m^2}{k_BT}\,\frac{\pi}{2}\,\frac{\tilde{\omega}}{(2|\sigma|)^3}\,\frac{(2\sigma)^2-(\tilde{\omega}-\xi)^2}{\mathcal{Z}}\exp\left(\frac{\tilde{\omega}^2-\xi^2}{4\sigma}\right), \tag{4.5}$$

where $\tilde{\omega}=\omega(m/\gamma k_BT)$, $\xi=mB/k_BT$, $\mathcal{Z}$ is the partition function (D3), and $\chi''_\perp(\omega)$ is nonzero in the interval $(\tilde{\omega}-\xi)^2\leqslant(2\sigma)^2$. (In order to compare this zero-damping formula with the numerical results, we write $\tilde{\omega}=\omega(2\lambda\tau_K\sigma)$, which for fixed $\omega\tau_K$, as it occurs in the plot, is a ''function'' of λ.) The lower panel of Fig. 9 shows that, for $\lambda=0.5$, Eq. (4.5) compares reasonably with the numerical results at intermediate-to-high temperatures, while the agreement extends to quite low temperatures already for $\lambda=0.1$.

Since Eq. (4.5) is a $\lambda=0$ formula, this comparison indicates that, in the intermediate-to-weak damping regime, the contribution of the spread of the precession frequencies of the magnetic moment to $\chi''_\perp(\omega)$ is sizable as compared to the

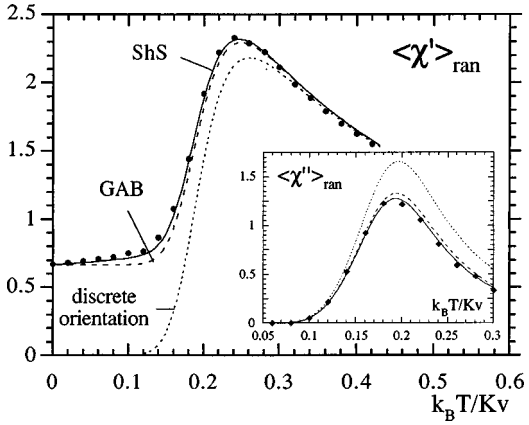

FIG. 10. $\langle \chi(\omega,T)\rangle_{\rm ran}$ vs T for $\omega\tau_K/2\pi=0.0025$, $B=0$, and $\lambda=0.1$ (symbols). The short-dashed line is for Eq. (D12), the medium-dashed line for Eq. (D11), and the solid lines for Eq. (D10). The integral relaxation time (D13) has been used for $\tau_\parallel$. For $\tau_\perp$, Eq. (D15) and $\tau_\perp=0$ have been employed (both results visually coincide).

effects of the damping. Therefore, by omitting that zero-damping effect one could erroneously extract values of λ from the $\chi''_\perp(\omega)$ data that overestimate the actual λ and, e.g., infer that the damping in superparamagnets is strong.

3. Response for anisotropy axes distributed at random

The comparison is finally effected for anisotropy axes distributed at random. In principle, this comparison could appear unnecessary due to the linearity of the response. Nevertheless, we shall carry it out since additional conclusions can be drawn.

First, as Fig. 10 shows, the discrete-orientation model is not able to yield the sizable low-temperature in-phase response, while the corresponding $\langle \chi''(T)\rangle_{\rm ran}$ overestimates the exact one. The curious point is the reasonable agreement of the Gittleman, Abeles, and Bozowski equation with the exact results for this anisotropy-axis distribution. Nevertheless, one should keep in mind that this agreement (as well as that of the discrete-orientation model at high temperatures), *originates from the cancellation of two faulty results for the longitudinal and transverse susceptibilities* (recall Figs. 8 and 9). Any departure of the anisotropy-axis distribution from random will show the limitations of such a model. Finally, as could be anticipated, the accord obtained between Eq. (D10) and the exact results is merely a consequence of the previously encountered agreements plus the linearity of the response. In addition, this accord is maintained even if we put $\tau_\perp=0$ in the transverse component of that equation (instantaneous transverse response), because the out-of-phase susceptibility is, at the frequencies considered, overwhelmingly dominated by the responses to the components of the probing field along the different anisotropy axes $[\langle \chi''(T)\rangle_{\rm ran}\simeq\frac{1}{3}\chi''_\parallel(T)]$. Note that this would also reasonably work for stronger damping since the thick dashed curve in Fig. 9, which is $\chi''_\perp(\omega,T)$ with the overdamped ($\lambda\gg1$) transverse relaxation time, works out an upper bound for $\chi''_\perp$ as a function of λ (specifically $\chi''_\perp\lesssim 5\times10^{-2}\mu_0 m^2/2Kv$).

Concerning the phase behavior, the fast intra-potential-well motions make a contribution to the transverse response much larger than to the longitudinal response. Therefore, as the former contribution is in some way accounted for by Eq. (D10), via the equilibrium transverse susceptibility, one finds that, inasmuch as $\langle\cos^2\alpha\rangle$ departs from unity, the Shliomis and Stepanov equation also describes the low-temperature phase shifts reasonably well (see the inset of Fig. 6).

V. DISCUSSION AND CONCLUSIONS

In this work, the stochastic Landau-Lifshitz-Gilbert equation (Brown-Kubo-Hashitsume model) has been integrated numerically, taking account of the differences of the stochastic calculus from the deterministic calculus. This Langevin-dynamics approach has been shown to be a useful tool in the study of the dynamics of magnetic nanoparticles.

When studying the long-time dynamics of the magnetic moments, the Langevin-dynamics method used requires an extensive computational effort and is then less efficient than numerical methods especially suitable for noninteracting spins, such as those based on continued-fraction techniques or the computation of the eigenvalues and amplitudes of the relevant dynamical modes by matrix methods.[7–11] However, with a significant increase of the computational effort, the Langevin-dynamics technique could also be used to study assemblies of interacting magnetic moments. In addition, the direct attainment of the time evolution (realizations) of the variables of the system, renders the Langevin-dynamics method unique as it directly yields the dynamics of the individual magnetic moments. This is especially relevant considering the current experiments on individual magnetic nanoparticles.[14]

In the study of the dynamics of individual magnetic moments, we have found interesting phenomena in the overbarrier rotation process, such as crossing-back and multiple crossing, which can be explained in terms of the gyromagnetic nature of the system. On the other hand, as a suitable probe of the intrinsic dynamics of the ensemble of magnetic moments, we have studied its linear dynamic susceptibility and set this in the context of the previously determined features of the individual dynamics. We have investigated the effect of the intra-potential-well relaxation modes on the low-temperature longitudinal dynamic response, showing their relatively small reflection in the $\chi_\parallel(\omega,T)$ curves (remarkably small in $\chi''_\parallel$) but their spectacular influence on the phase shifts. On the other hand, the sizable contribution of the spread of the precession frequencies of the magnetic moment in the anisotropy field to the out-of-phase transverse response at intermediate-to-high temperatures, has been demonstrated by comparing the numerical results with the exact zero-damping expression for $\chi''_\perp(\omega)$. Accounting for this effect may be relevant to properly assess the strength of the damping in superparamagnetic systems.

We have also compared the numerical results with heuristic analytical expressions. It has been demonstrated that both the discrete-orientation and the Gittleman, Abeles, and Bozowski equations fail to describe the exact results, whereas the simple formula proposed by Shliomis and Stepanov (sum of two Debye-type relaxation mechanisms) matches the coarse features of the susceptibility reasonably. In addition, owing to the fact that the intra-potential-well relaxation modes are very fast and, thus, $\chi''_\parallel$ is well described by Eq.

(D10) (see the inset of Fig. 8), while $\chi_\perp''$ is relatively small, the theoretical background of the methods of determination of the energy-barrier (Kv) distribution that are based on the use of the *out-of-phase* component of the Shliomis and Stepanov equation (with $\omega\tau_\perp = 0$),[16,17] is supported in the context of the Brown-Kubo-Hashitsume stochastic model.

Finally, since the frequencies considered here (in the MHz range) are much lower than those where resonant behavior occurs, the results obtained for the averaged quantities would be valid in the usual frequency range of experiments on small magnetic particles (say $\omega/2\pi \sim 10^{-2}$–10^4 Hz). In addition, the large value of the effective τ_0 ($\sim 10^{-8}$–10^{-7} s) in the Arrhenius law $\tau_\parallel \simeq \tau_0 \exp(\Delta U/k_B T)$, encountered in molecular magnetic clusters having high spin in their ground state, entails that experimental conditions with $\omega/2\pi \sim 10^3$–10^4 Hz already correspond to the frequency range considered in this work. Indeed, these systems neatly exhibit the qualitative features encountered for the linear dynamic susceptibility at ''high'' (but below ferromagnetic resonance) frequencies (see Refs. 32 and 33 for Fe_8 and Mn_{12}, respectively): wide maxima in $\chi(\omega,T)$ vs T for only one potential barrier (relaxation time), sizable $\chi'(T)$ at temperatures well below the blocking temperatures, and flattening of the peak of $\chi''(T)$ with increasing ω.

ACKNOWLEDGMENTS

The authors are grateful to F. Falo and J. M. Sancho for invaluable advice in the early stages of this work, and to D. A. Garanin for a critical reading of the manuscript and valuable suggestions.

APPENDIX A: DETERMINISTIC DYNAMICS

In this appendix, we shall investigate solutions of the Landau-Lifshitz equation in the absence of fluctuations,

$$\frac{d\vec{m}}{dt} = \gamma \vec{m} \wedge \vec{B}_{\rm eff} - \gamma \frac{\lambda}{m} \vec{m} \wedge (\vec{m} \wedge \vec{B}_{\rm eff}), \tag{A1}$$

restricting our attention to the case where the Hamiltonian of $\vec{m}$ is axially symmetric. On examining Eq. (2.9), one concludes that the physical range where the fluctuations play a minor role is the low-temperature range, in the sense that $\tau_N^{-1} \ll \gamma |\vec{B}_{\rm eff}|$ [i.e., $2\lambda k_B T \ll m |\vec{B}_{\rm eff}|$; see Eq. (2.6)].

1. General solution for axially symmetric Hamiltonians

For an axially symmetric Hamiltonian, $\vec{B}_{\rm eff}(\vec{m})$ is parallel to the symmetry axis, which can be chosen as the z axis, $\vec{B}_{\rm eff} = B_{\rm eff}(\vec{m})\hat{z}$. Then, on introducing the $\vec{m}$-dependent ''frequency'' $\omega_{\rm eff}(\vec{m}) = \gamma B_{\rm eff}(\vec{m})$, we can explicitly write the deterministic Landau-Lifshitz equation (A1) as a system of coupled ordinary differential equations:

$$\frac{dm_x}{dt} = \omega_{\rm eff}\left(m_y - \frac{\lambda}{m} m_x m_z \right),$$

$$\frac{dm_y}{dt} = \omega_{\rm eff}\left(-m_x - \frac{\lambda}{m} m_y m_z \right),$$

$$\frac{dm_z}{dt} = \omega_{\rm eff} \frac{\lambda}{m} (m^2 - m_z^2).$$

Next, on introducing spherical coordinates $m_x + i m_y = m \sin\vartheta \exp(-i\varphi)$ and $m_z = m\cos\vartheta$ (we measure the azimuthal angle clockwise), the above system of differential equations can equivalently be written as

$$\frac{d\vartheta}{dt} = -\lambda \omega_{\rm eff} \sin\vartheta, \tag{A2}$$

$$\frac{d\varphi}{dt} = -\frac{1}{\lambda \sin\vartheta} \frac{d\vartheta}{dt}, \quad (\text{or } d\varphi/dt = \omega_{\rm eff}). \tag{A3}$$

Equation (A3) can be solved by separation of variables, yielding

$$\varphi(\vartheta) - \varphi(\vartheta_0) = -\frac{1}{\lambda} \ln\left(\tan\frac{\vartheta}{2} \Big/ \tan\frac{\vartheta_0}{2} \right), \tag{A4}$$

where $\vartheta_0 = \vartheta(t_0)$, t_0 being the initial time. Because $\omega_{\rm eff} = \omega_{\rm eff}(\vartheta)$, we can also separate the variables in Eq. (A2) to get the following implicit expression for $\vartheta(t)$:

$$-\lambda(t - t_0) = \int_{\vartheta_0}^{\vartheta(t)} \frac{d\vartheta'}{\omega_{\rm eff}(\vartheta') \sin\vartheta'}. \tag{A5}$$

Equations (A4) and (A5) are the solution of the deterministic Landau-Lifshitz equation for *any* axially symmetric Hamiltonian $\mathcal{H}(\vartheta)$.

2. The simplest axially symmetric Hamiltonian

Let us now specialize the above general solutions to the Hamiltonian obtained by the sum of the simplest axially symmetric anisotropy potential plus a longitudinal Zeeman term. Then [cf. Eq. (3.2)]

$$\vec{B}_{\rm eff} = B\hat{z} + (B_K/m)(\vec{m}\cdot\hat{z})\hat{z}, \tag{A6}$$

and $\omega_{\rm eff}(\vec{m}) = \gamma B_{\rm eff}(\vec{m})$ can be written as

$$\omega_{\rm eff}(\vartheta) = \omega_B + \omega_K \cos\vartheta, \quad \omega_B = \gamma B, \quad \omega_K = \gamma B_K, \tag{A7}$$

while the integral in the solution (A5) is given by

$$\int \frac{d\vartheta}{(\omega_B + \omega_K \cos\vartheta)\sin\vartheta}$$

$$= \frac{1}{\omega_B + \omega_K} \ln\left(\tan\frac{\vartheta}{2} \right) + \frac{\omega_K}{\omega_B^2 - \omega_K^2} \ln(\omega_B + \omega_K)$$

$$+ \frac{\omega_K}{\omega_B^2 - \omega_K^2} \ln\left[1 + \left(\frac{\omega_B - \omega_K}{\omega_B + \omega_K} \right) \tan^2\frac{\vartheta}{2} \right].$$

Therefore, from the general result (A5) we get

$$C e^{-\lambda(\omega_B + \omega_K)t} = \tan\frac{\vartheta}{2} \left[1 + \left(\frac{\omega_B - \omega_K}{\omega_B + \omega_K} \right) \tan^2\frac{\vartheta}{2} \right]^{\omega_K/(\omega_B - \omega_K)}, \tag{A8}$$

where the constant of integration C involves both the terms evaluated at $t=t_0$ and the second term on the right-hand side of the above integral, which is a constant too.

Particular cases

The above implicit solution for $\vartheta(t)$ turns into an explicit one in various special situations.

a. Dynamics in the absence of the anisotropy energy. Here $\omega_K=0$, so that Eqs. (A4) and (A8) reduce to the celebrated results $[\varphi_0=\varphi(t_0)]$

$$\tan\frac{\vartheta}{2}=\tan\frac{\vartheta_0}{2}e^{-\lambda\omega_B(t-t_0)},\quad \varphi(t)-\varphi_0=\omega_B(t-t_0).$$

Thus, the motion of $\vec{m}$ consist of a precession with frequency $\omega_B=\gamma B$ about $\hat{z}$ and a spiraling towards this axis with a characteristic time constant [cf. Eq. (3.4)]

$$\tau_B=\frac{1}{\lambda\omega_B}=\frac{1}{\lambda\gamma B}. \tag{A9}$$

b. Dynamics in the absence of an external field. Here $\omega_B=0$, so that, by using $\tan\vartheta=2\tan(\vartheta/2)/[1-\tan^2(\vartheta/2)]$ in Eq. (A8), one gets

$$\tan\vartheta=\tan\vartheta_0 e^{-\lambda\omega_K(t-t_0)}. \tag{A10}$$

Thus, the spiraling towards the minima ($K>0$ case) has a characteristic time [Eq. (3.4)]

$$\tau_K=\frac{1}{\lambda\omega_K}=\frac{1}{\lambda\gamma B_K}. \tag{A11}$$

For easy-plane anisotropy ($K<0$) one has $B_K,\omega_K<0$, so that $\lim_{t\to\infty}\tan\vartheta=\infty$, that is, $\vartheta\to\pi/2$ as $t\to\infty$, and the magnetic moment eventually rests in the equatorial plane.

Concerning the azimuthal angle, by expressing $\tan(\vartheta/2)$ in terms of $\tan\vartheta$, one gets from Eq. (A4)

$$\varphi(t)-\varphi_0=\omega_K(t-t_0)-\frac{1}{\lambda}\ln\left[\frac{1+\sec\vartheta_0}{1\pm\sqrt{1+\tan^2\vartheta_0 e^{-2\lambda\omega_K(t-t_0)}}}\right],$$

where the plus sign corresponds to $\vartheta\in[0,\pi/2]$ and the minus sign to $\vartheta\in[\pi/2,\pi]$. From this equation it follows that the asymptotic $\lambda|\omega_K|(t-t_0)\gg1$ behavior of the azimuthal angle for $K>0$ is

$$\varphi(t)-\varphi_0\simeq\pm\left[\omega_K(t-t_0)-\frac{1}{\lambda}\ln\left(\frac{1\pm\sec\vartheta_0}{2}\right)\right],$$

which corresponds to a precession close to the bottom of the corresponding potential well with an angular velocity $\omega_K\hat{z}$ in the $z>0$ well and $-\omega_K\hat{z}$ in the $z<0$ well. For easy-plane anisotropy ($K<0$), one finds from Eq. (A4) that the magnetic moment finally rests in the equatorial plane at $\varphi-\varphi(\vartheta_0)=1/\lambda\ln[\tan(\vartheta_0/2)]$ (unless it starts at $\vartheta_0=0,\pi$, which are unstable equilibrium points).

c. Dynamics close to the potential minima (case $B_K>0$). Let us initially assume $\vartheta\simeq0$ (i.e., $\tan(\vartheta/2)\ll1$). Then, on retaining terms of order $\tan(\vartheta/2)$ in Eq. (A8), we get $\tan(\vartheta/2)\simeq\tan(\vartheta_0/2)\exp[-\lambda(\omega_B+\omega_K)(t-t_0)]$ and $\varphi(t)-\varphi_0\simeq(\omega_B+\omega_K)(t-t_0)$ by Eq. (A4). However, within the same approximation ($\vartheta\ll1$) we can replace the tangents by their arguments, getting

$$\vartheta(t)\simeq\vartheta_0 e^{-\lambda(\omega_B+\omega_K)(t-t_0)},\quad \varphi(t)-\varphi_0\simeq(\omega_B+\omega_K)(t-t_0).$$

Thus, $\vec{m}$ precesses with frequency $\omega_B+\omega_K$ when spiraling towards the $\vartheta=0$ potential minimum and the time constant of the decay of ϑ is $1/[\lambda(\omega_B+\omega_K)]=\tau_B\tau_K/(\tau_B+\tau_K)$. Note that the characteristic decay time of $m_z\propto\cos\vartheta\simeq1-\vartheta^2/2$, is a half of this result. Moreover the approximation used is self-consistent if $\omega_B+\omega_K>0$, that is, if the $\vartheta=0$ potential minimum exists.

We shall finally consider the $\vartheta\simeq\pi$ case. In this situation $\vartheta/2\simeq\pi/2$ and, hence, $\tan(\vartheta/2)\gg1$, so we can use $1\ll(\omega_B-\omega_K)/(\omega_B+\omega_K)\tan^2(\vartheta/2)$ in Eq. (A8), to get $\tan(\vartheta/2)\simeq\tan(\vartheta_0/2)\exp[\lambda(\omega_K-\omega_B)(t-t_0)]$ and then $\varphi(t)-\varphi_0\simeq-(\omega_K-\omega_B)(t-t_0)$ by Eq. (A4). However, for $\tan(\vartheta/2)\gg1$, one has $\tan\vartheta\simeq-2/\tan(\vartheta/2)$, and by expanding $\tan\vartheta$ about $\vartheta=\pi$, we finally get

$$\vartheta(t)-\pi\simeq(\vartheta_0-\pi)e^{-\lambda(\omega_K-\omega_B)(t-t_0)},$$

$$\varphi(t)-\varphi_0\simeq-(\omega_K-\omega_B)(t-t_0).$$

Therefore, $\vec{m}$ precesses with frequency $\omega_K-\omega_B$ (about $-\hat{z}$) when spiraling towards the $\vartheta=\pi$ minimum, while ϑ decays with a characteristic time constant $1/[\lambda(\omega_K-\omega_B)]=\tau_B\tau_K/(\tau_B-\tau_K)$ (and m_z with half of this value). Note finally that, the approximation used is self-consistent if $\omega_K-\omega_B>0$, i.e., when the $\vartheta=\pi$ minimum exists.

APPENDIX B: DERIVATION OF THE FOKKER-PLANCK EQUATIONS

Let us consider the general system of Langevin equations

$$\frac{dy_i}{dt}=A_i(\mathbf{y},t)+\sum_k B_{ik}(\mathbf{y},t)L_k(t), \tag{B1}$$

where $\mathbf{y}=(y_1,\ldots,y_n)$ (the variables of the system), k runs over a given set of indices, and the ''Langevin'' sources $L_k(t)$ are (independent) Gaussian stochastic processes satisfying

$$\langle L_k(t)\rangle=0,\quad \langle L_k(t)L_{\ell}(s)\rangle=2D\delta_{k\ell}\delta(t-s).$$

When the functions $B_{ik}(\mathbf{y},t)$ depend on $\mathbf{y}$, the noise in the above equations is termed ''multiplicative,'' whereas for $\partial B_{ik}/\partial y_j\equiv0$ the noise is called ''additive'' (here the Itô and Stratonovich stochastic calculi coincide).

The time evolution of $P(\mathbf{y},t)$, the nonequilibrium probability distribution for $\mathbf{y}$ at time t, is given by the Fokker-Planck equation

$$\frac{\partial P}{\partial t}=-\sum_i\frac{\partial}{\partial y_i}\left[\left(A_i+D\sum_{jk}B_{jk}\frac{\partial B_{ik}}{\partial y_j}\right)P\right]+\sum_{ij}\frac{\partial^2}{\partial y_i\partial y_j}\left[\left(D\sum_k B_{ik}B_{jk}\right)P\right],$$

where the Stratonovich calculus has been used[19] to treat the (in general) multiplicative fluctuating terms in the Langevin

equations (B1) [when using the Itô calculus the *noise-induced* drift coefficient $D\Sigma_{jk}B_{jk}(\partial B_{ik}/\partial y_j)$ is omitted]. On taking the y_j derivatives of the second term on the right-hand side, one alternatively gets the Fokker-Planck equation in the form of a continuity equation for the probability distribution, namely,

$$\frac{\partial P}{\partial t}=-\sum_i \frac{\partial}{\partial y_i}\left\{\left[A_i-D\sum_k B_{ik}\left(\sum_j \frac{\partial B_{jk}}{\partial y_j}\right)-D\sum_{jk} B_{ik}B_{jk}\frac{\partial}{\partial y_j}\right]P\right\}. \tag{B2}$$

Next, on considering the *stochastic Landau-Lifshitz-Gilbert equation* (2.1), supplemented by the statistical properties (2.3), the following substitutions cast them into the form of the general system of Langevin equations (B1): $(y_1,y_2,y_3)=(m_x,m_y,m_z)$, $L_k(t)=b_{\mathrm{fl},k}(t)$, and

$$A_i=\gamma\left[\vec{m}\wedge\vec{B}_{\mathrm{eff}}-\frac{\lambda}{m}\vec{m}\wedge(\vec{m}\wedge\vec{B}_{\mathrm{eff}})\right]_i, \tag{B3}$$

$$B_{ik}=\gamma\left[\sum_j \epsilon_{ijk}m_j+\frac{\lambda}{m}(m^2\delta_{ik}-m_im_k)\right], \tag{B4}$$

where ϵ_{ijk} is the totally antisymmetrical unit tensor (Levi-Civita symbol) and we have expanded the triple vector product $-\vec{m}\wedge(\vec{m}\wedge\vec{b}_{\mathrm{fl}})=m^2\vec{b}_{\mathrm{fl}}-\vec{m}(\vec{m}\cdot\vec{b}_{\mathrm{fl}})$. Note that the B_{ik} depend on $\vec{m}$, i.e., *the noise terms in the stochastic Landau-Lifshitz-Gilbert equation are multiplicative*.

On using

$$\frac{\partial B_{ik}}{\partial m_j}=\gamma\left[\epsilon_{ijk}+\frac{\lambda}{m}(2\delta_{ik}m_j-\delta_{ij}m_k-\delta_{kj}m_i)\right] \tag{B5}$$

($\lambda/m=\eta\gamma/v$ has not been differentiated since it is a constant independent of $\vec{m}$) and accounting for $\epsilon_{jjk}=0$, one finds $\Sigma_j\partial B_{jk}/\partial m_j=-2(\gamma\lambda/m)m_k$, from which we get $\Sigma_k B_{ik}(\Sigma_j\partial B_{jk}/\partial m_j)=0$ by Eq. (B4). Therefore, the second term on the right-hand side of the general Fokker-Planck equation (B2) vanishes identically in this case. For the third term, by repeated use of $(\vec{J}\wedge\vec{J}')_i=\Sigma_{rs}\epsilon_{irs}J_rJ'_s$, we get

$$-D\sum_{jk} B_{ik}B_{jk}\frac{\partial P}{\partial m_j}=\frac{1}{2\tau_{\mathrm{N}}}\left[\vec{m}\wedge\left(\vec{m}\wedge\frac{\partial P}{\partial\vec{m}}\right)\right]_i, \tag{B6}$$

where $\tau_{\mathrm{N}}^{-1}=2D\gamma^2(1+\lambda^2)$ is the Néel (free-diffusion) time. On introducing these results into Eq. (B2) one finally arrives at the Fokker-Planck equation (2.5).

Likewise, when one considers the *stochastic Landau-Lifshitz equation* (2.4), supplemented by Eqs. (2.3), the expression for A_i is identical with Eq. (B3), whereas B_{ik} reduces to (in this case there are Langevin fields in the precession term only)

$$B_{ik}=\gamma\sum_j \epsilon_{ijk}m_j. \tag{B7}$$

Therefore, $\partial B_{ik}/\partial m_j$ simplifies to $(\partial B_{ik}/\partial m_j)=\gamma\epsilon_{ijk}$ [cf. Eq. (B5)], so that one again gets that the second term in the general Fokker-Planck equation (B2) vanishes (here $\partial B_{jk}/\partial m_j\equiv 0$ by $\epsilon_{jjk}=0$). On the other hand, on introducing the reduced expression $\tau_{\mathrm{N}}^{-1}=2D\gamma^2$ for the Néel time, the third term in Eq. (B2) can also be cast into the form (B6).

Thus, the Fokker-Planck equations associated with both the stochastic Landau-Lifshitz-Gilbert equation (2.1) *and the stochastic Landau-Lifshitz equation* (2.4) *are given by Eq.* (2.5)*, the only difference being the relation between the Néel time and the amplitude of the fluctuating field:*

$$\frac{1}{\tau_{\mathrm{N}}}=\begin{cases}2D\gamma^2(1+\lambda^2) & \text{(LLG)},\\ 2D\gamma^2 & \text{(LL)}.\end{cases} \tag{B8}$$

APPENDIX C: NUMERICAL METHOD

1. Numerical integration scheme

On using the dimensionless quantities introduced in Sec. III [Eqs. (3.3) and (3.4)], the stochastic Landau-Lifshitz-Gilbert equation (2.1), can be rewritten in a dimensionless form suitable for computation, namely,

$$\frac{d\vec{e}}{d\overline{t}}=\frac{1}{\lambda}\vec{e}\wedge[\vec{h}_{\mathrm{eff}}+\vec{h}_{\mathrm{fl}}(\overline{t})]-\vec{e}\wedge\{\vec{e}\wedge[\vec{h}_{\mathrm{eff}}+\vec{h}_{\mathrm{fl}}(\overline{t})]\}, \tag{C1}$$

where $\vec{e}=\vec{m}/m$ is a unit vector in the direction of the magnetic moment and the statistical properties of $\vec{h}_{\mathrm{fl}}(\overline{t})$, which arise directly from those of $\vec{b}_{\mathrm{fl}}(t)$ [Eqs. (2.3)], are

$$\langle h_{\mathrm{fl},i}(\overline{t})\rangle=0, \tag{C2}$$

$$\langle h_{\mathrm{fl},i}(\overline{t})h_{\mathrm{fl},j}(\overline{s})\rangle=2\left(\frac{\lambda^2}{1+\lambda^2}\frac{k_{\mathrm{B}}T}{2Kv}\right)\delta_{ij}\delta(\overline{t}-\overline{s}), \tag{C3}$$

where we have used Eq. (2.7) for D and $\delta(t)=\delta(\overline{t})d\overline{t}/dt=\delta(\overline{t})\tau_K^{-1}$ [the factor in the brackets is indeed $D/(\tau_K B_K^2)$]. Next, let us cast the dimensionless Eq. (C1) into the form of the general system of Langevin equations (B1) by setting $L_i=h_{\mathrm{fl},i}$ and introducing [cf. Eqs. (B3) and (B4)]

$$A_i=\sum_k\left[\frac{1}{\lambda}\sum_j \epsilon_{ijk}e_j+(\delta_{ik}-e_ie_k)\right]h_{\mathrm{eff},k}, \tag{C4}$$

$$B_{ik}=\frac{1}{\lambda}\sum_j \epsilon_{ijk}e_j+(\delta_{ik}-e_ie_k). \tag{C5}$$

[For the corresponding dimensionless stochastic Landau-Lifshitz equation $B_{ik}=\lambda^{-1}\Sigma_j\epsilon_{ijk}e_j$ [cf. Eq. (B7)], while $(\lambda^2/1+\lambda^2)(k_BT/2Kv)\to\lambda^2(k_BT/2Kv)$ in Eq. (C3).]

Concerning the choice of the numerical integration scheme, one must keep in mind that the noise terms in Eq. (C1) are multiplicative (B_{ik} depends on $\vec{e}$). Together with difficulties at the level of definition, the occurrence of multiplicative white noise in a Langevin equation entails some technical problems as well. For instance, serious difficulties arise in developing high-order numerical integration schemes for this case.[34] In general, the mere translation of a numerical scheme valid for deterministic differential equations does not necessarily yield a proper scheme in the stochastic case: (i) Depending on the original deterministic scheme chosen, its

naïve stochastic translation might converge to an Itô solution, to a Stratonovich solution, or to none of them. (ii) Even if there exists proper convergence of the scheme chosen in the context of the stochastic calculus used, the order of convergence is usually lower than that of the original deterministic scheme.

Let us consider the stochastic generalization of the deterministic Heun scheme, namely,

$$y_i(t+\Delta t)=y_i(t)+\tfrac{1}{2}[A_i(\tilde{\mathbf{y}},t+\Delta t)+A_i(\mathbf{y},t)]\Delta t + \tfrac{1}{2}\sum_k [B_{ik}(\tilde{\mathbf{y}},t+\Delta t)+B_{ik}(\mathbf{y},t)]\Delta W_k , \tag{C6}$$

where Δt is the discretization time interval, $\mathbf{y}=\mathbf{y}(t)$, the $\tilde{y}_i$ are Euler-type supporting values,

$$\tilde{y}_i=y_i(t)+A_i(\mathbf{y},t)\Delta t+\sum_k B_{ik}(\mathbf{y},t)\Delta W_k , \tag{C7}$$

and the $\Delta W_k=\int_t^{t+\Delta t} ds L_k(s)$ are Gaussian random numbers the first two moments of which are

$$\langle \Delta W_k\rangle=0, \quad \langle \Delta W_k \Delta W_{k'}\rangle=(2D\Delta t)\delta_{kk'}. \tag{C8}$$

The stochastic Heun scheme (C6) converges *in quadratic mean* to the solution of the general system of stochastic differential equations (B1) *when interpreted in the sense of Stratonovich*.[35] On the other hand, if one uses the Euler-type Eq. (C7) as the numerical integration scheme [by identifying $y_i(t+\Delta t)=\tilde{y}_i$], the constructed trajectory *converges to the Itô solution* of the same system of equations (B1) (see, e.g., Ref. 35). A proper Euler-type scheme in the context of the Stratonovich stochastic calculus is obtained when the deterministic drift in Eq. (C7), A_i, is augmented by the noise-induced drift, namely,

$$y_i(t+\Delta t)=y_i(t)+\left[A_i+D\sum_{jk} B_{jk}\frac{\partial B_{ik}}{\partial y_j}\right]_{(\mathbf{y},t)}\Delta t + \sum_k B_{ik}(\mathbf{y},t)\Delta W_k . \tag{C9}$$

We note in passing that the noise-induced drift for Eq. (C1) is $(\lambda^2/1+\lambda^2)(k_BT/2Kv)\Sigma_{jk}B_{jk}\partial B_{ik}/\partial e_j=-(k_BT/Kv)e_i=-(\tau_K/\tau_N)e_i$ [which corresponds to the term $-\langle\vec{m}\rangle/\tau_N$ in the averaged dynamical equation (2.9)].

For *commutative noise*, defined by

$$\sum_j B_{jk}\frac{\partial B_{ik'}}{\partial y_j}=\sum_j B_{jk'}\frac{\partial B_{ik}}{\partial y_j}, \quad \forall i \tag{C10}$$

(i.e., symmetry with respect to the subscripts k and k'), the stochastic Heun scheme has an order of convergence higher than that of the Euler scheme (C9).[35] The condition of commutative noise is rather general and includes additive noise, $\partial B_{ik'}/\partial y_j\equiv 0$, diagonal multiplicative noise, $B_{ij}(\mathbf{y},t)=\delta_{ij}B_{ii}(y_i)$, and linear multiplicative noise, $B_{ij}(\mathbf{y},t)=B_{ij}(t)y_i$ (see, e.g., Ref. 34, p. 348). Although the multiplicative noise in the stochastic Landau-Lifshitz-Gilbert equation is *noncommutative* (the same holds for the stochastic Landau-Lifshitz equation; we omit the corresponding proofs), we shall employ the stochastic Heun method (C6) to integrate Eq. (C1) numerically. This is done because: (i) The Heun scheme yields Stratonovich solutions of the stochastic differential equations naturally, without alterations to the drift term and (ii) the deterministic part of the differential equations is treated with a second order accuracy in Δt, which renders the Heun scheme numerically more stable than the Euler-type schemes.

Previous approaches. In order to integrate the stochastic Landau-Lifshitz-Gilbert equation numerically, Lyberatos and Chantrell[13] unfortunately used a bare Euler scheme analogous to Eq. (C7), which omits the noise-induced drift, instead of using the Stratonovich Euler scheme (C9). Inasmuch as Eq. (C7) yields Itô solutions of the stochastic differential equations and, in contrast, they employed a relation between the amplitude of the thermal-agitation field and T equivalent to Eq. (2.7) (which pertains to the Stratonovich stochastic calculus), their approach is not consistent. Even the stationary properties that could be derived by means of such an approach would not coincide with the proper thermal-equilibrium properties (recall the discussion in Sec. II). Similar considerations hold for the numerical approach of Ref. 36, where a deterministic backward Euler method was simply used to deal with the stochastic Landau-Lifshitz-Gilbert equation. In contrast, a rigorous numerical treatment of the multiplicative noise terms of the stochastic Landau-Lifshitz equation has recently been effected by Antropov, Tretyakov, and Harmon,[37] by means of a Runge-Kutta method suitable for systems with *weak* noise.

2. Implementation

The integration of the stochastic Landau-Lifshitz-Gilbert equation is performed by starting from a given initial configuration, and updating recursively the state of the system, $\vec{m}(t)\rightarrow\vec{m}(t+\Delta t)$, by means of the set of finite-difference equations (C6). This generates stochastic trajectories from which, when required, averages are directly computed. When one extrapolates the results obtained to zero discretization time interval Δt, the only error in the *averaged* quantities is a statistical error bar that can, in principle, be made arbitrarily small by averaging over a sufficiently large number of stochastic trajectories. We do not carry out such a $\Delta t\rightarrow 0$ limiting procedure but we employ a discretization time interval small enough. We use $\Delta t=0.01\tau_K$ throughout [that is $\Delta\bar{t}=0.01$; see Eq. (3.4)], except for damping coefficients $\lambda\gtrsim 0.5$, where we employ $\Delta t=0.0025\tau_K$.

The *Gaussian* random numbers required to simulate the ΔW_k occurring in Eq. (C6), are constructed from *uniformly* distributed ones by means of the Box-Muller algorithm (Ref. 38, p. 280). As a large amount of uniform random numbers is used, we have chosen the subroutine RAN2 of Ref. 38, p. 272, to generate them. This subroutine has period $\sim 10^{18}$, so artifacts associated with period exhaustion are safely avoided. On the other hand, since the generation of the random numbers is the slowest step in the recursive scheme, when computing a quantity at various temperatures we generate all the trajectories at once, by using the same sequence of random numbers for the different temperatures.

When computing average quantities, in order to minimize effects that are not caused by the application of the probing field $\Delta\vec{B}(t)$, the following method is used. Starting from the same initial configuration, the equations of motion are solved for two identical systems, one in the presence of $\Delta\vec{B}(t)$ and the other subjected to $-\Delta\vec{B}(t)$, and the time evolution analyzed is that of $\vec{m}(t)=\frac{1}{2}\{\vec{m}[\Delta\vec{B}(t)]-\vec{m}[-\Delta\vec{B}(t)]\}$. Moreover, we have found that this *subtraction technique* significantly diminishes the number of stochastic trajectories required to achieve convergence in the computed results. On the other hand, as long as one applies a *finite* probing field when computing the linear dynamic response of the ensemble of spins, the possibility of encountering nonlinear effects in the response arises. Along with the precautions described below, the subtraction procedure automatically eliminates the nonlinear terms *quadratic* in the probing field that occur when a bias field is applied.

3. Statistical errors and optimization

When computing the dynamic response of the ensemble, the system of spins is subjected to a probing field $\Delta\vec{B}(t)=\Delta\vec{B}_0\cos(\omega t)$. Statistical errors occur in the computed quantities because one makes a finite number $N_{\rm m}$ of statistically independent ''measurements'' on the system. By the outcome of one such measurement is meant a quantity computed during, e.g., a cycle of the oscillating field,

$$Q_n=\int_n dt f[\vec{m}_1(t),\ldots,\vec{m}_N(t)]g(t), \tag{C11}$$

where the index n denotes integration over the nth cycle, N is the number of spins in the system, and $g(t)$ is a function of the time, typically a sinusoidal function of ωt. The same notation can be maintained when considering the computation of thermal-equilibrium quantities; in this case the integral is carried over a ''measurement'' time interval $t_{\rm m}$ and $g(t)=1/t_{\rm m}$.

An estimation of the exact result is given by

$$q=\frac{1}{N_{\rm m}}\sum_{n=1}^{N_{\rm m}} Q_n. \tag{C12}$$

The quantities q and Q are characterized by probability distributions whose ℓth-order cumulants κ_ℓ are related by $\kappa_\ell(q)=N_{\rm m}^{-(\ell-1)}\kappa_\ell(Q)$ (see, e.g., Ref. 39). Therefore, the moments required to evaluate these cumulants are $\overline{Q^\ell}=N_{\rm m}^{-1}\Sigma_{n=1}^{N_{\rm m}}(Q_n)^\ell$, which can be computed at the same time with $q=\overline{Q}$. For large $N_{\rm m}$, because the q distribution is Gaussian to a good approximation, the *result of the simulation* is taken as the interval $(q-[\kappa_2(q)]^{1/2},q+[\kappa_2(q)]^{1/2})$, in the sense that the exact value lies within this interval with probability 0.68, with $2[\kappa_2(q)]^{1/2}$ being the corresponding *statistical error*. Accordingly, a relevant parameter for the computed quantity is its *relative fluctuation*, defined as $\delta q/q\equiv[\kappa_2(q)]^{1/2}/q$ (standard deviation over mean value). From the above relation between $\kappa_\ell(q)$ and $\kappa_\ell(Q)$ one gets $\delta q/q=N_{\rm m}^{-1/2}\delta Q/Q$, where $\delta Q/Q=[\kappa_2(Q)]^{1/2}/\overline{Q}$ is the relative fluctuation of Q. The following considerations on the computation of the thermal-equilibrium response will suggest a way to decrease $\delta q/q$ more efficiently than to further increase the number of measurements, which is not very efficient because of the occurrence of the square root $N_{\rm m}^{-1/2}$ in the denominator of the above expression for $\delta q/q$.

Thermal-equilibrium response. If the field-dependent part of the energy depends on $\vec{B}$ via $-\Sigma\vec{m}\cdot\vec{B}$, on assuming $\vec{B}\|\hat{z}$ and defining $m_{z,\rm tot}=\Sigma\vec{m}\cdot\hat{z}$, where the sums are taken over the spins of the system, we know from statistical mechanics that the relation

$$\frac{\partial}{\partial B}\langle m_{z,\rm tot}\rangle_0=\frac{1}{k_{\rm B}T}[\langle m_{z,\rm tot}^2\rangle_0-\langle m_{z,\rm tot}\rangle_0^2], \tag{C13}$$

where $\langle\rangle_0$ denotes thermal-equilibrium average, holds irrespective of the magnitude of $\vec{B}$. Therefore, on defining the magnetization in the field direction, M_z, as the time average of the magnetic moment *per spin*, $M_{z,n}=\int_n dt m_{z,\rm tot}(t)/(t_{\rm m}N)$ (M_z plays the role of the Q above), and identifying the statistical distribution of $M_{z,n}$ with the statistical-mechanical distribution, one can write

$$\frac{\delta M_z}{M_z}=\frac{1}{(t_{\rm m}N)^{1/2}}\frac{\sqrt{k_{\rm B}T\partial M_z/\partial B}}{M_z}. \tag{C14}$$

Note that, concerning the computation of averages, the factor $(t_{\rm m}N)^{-1/2}$ in Eq. (C14) plays a role akin to that of $N_{\rm m}^{-1/2}$ above. Thus, to further enlarge $t_{\rm m}$ or N is as effective as to enlarge $N_{\rm m}$ to optimize the simulation. Nevertheless, for rather general functional dependences of M_z on B, the quantity $\sqrt{k_{\rm B}T\partial_B M_z}/M_z$ (and hence $\delta M_z/M_z$) decreases with increasing B. Consequently, if one is interested in the computation of, e.g., the equilibrium linear susceptibility $\chi(T)$, one can apply the largest probing field without leaving the linear response range ($M_z\propto\chi\Delta B_0$) and then compute M_z. This procedure significantly reduces $\delta M_z/M_z$ and, thus, the statistical errors of the quantities computed, so that the calculations are optimized.

Let us finally estimate the temperature-dependent range where $M_z\propto\Delta B_0$ holds when the system has the simplest axially symmetric anisotropy potential [see Eq. (3.1)]. On assuming a zero bias field and a static *probing* field, one has $M_z=M_z(\sigma,\Delta\xi_0;\alpha)$, where α is the angle between the anisotropy axis and the probing field, $\sigma=Kv/k_{\rm B}T$, and $\Delta\xi_0=m\Delta B_0/k_{\rm B}T$. The magnetic anisotropy causes the crossover from the $\sigma\ll1$, free-rotator (Langevin) regime, where $M_z\simeq m[\coth(\Delta\xi_0)-(\Delta\xi_0)^{-1}]$, to the discrete-orientation (Ising) regime, where $M_z\simeq(m\cos\alpha)\tanh(\Delta\xi_0\cos\alpha)$, for large σ (low temperatures). The narrower linear range occurs for the last functional dependence when $\cos\alpha=1$, since $M_z\simeq m\cos^2\alpha\Delta\xi_0$ holds up to $(\Delta\xi_0\cos\alpha)\simeq0.3$. Hence, we can scale the probing field with T according to $m\Delta B_0=0.3k_{\rm B}T$ ($\Delta\xi_0\simeq0.3$), which ensures that at higher temperatures, where the linear range is somewhat wider (for $\sigma\ll1$, $M_z\simeq\frac{1}{3}m\Delta\xi_0$ up to $\Delta\xi_0\simeq0.5$), the response still lies in the linear response range.

These considerations, which apply to the computation of thermal-equilibrium quantities, suggest that the same procedure could be tried in the calculation of the dynamical quan-

tities. In the averages computed in this work, this method dramatically improves the efficiency of the simulations.

APPENDIX D: MODELS FOR THE LINEAR DYNAMIC RESPONSE

In this appendix we shall review, and in some cases generalize, various expressions that have been proposed to describe the $\chi(\omega)$ of independent magnetic nanoparticles.

1. Equilibrium quantities

In order to write down the equilibrium quantities that occur in the expressions discussed below, it is convenient to introduce the dimensionless anisotropy-barrier and field parameters

$$\sigma=\frac{Kv}{k_{\mathrm{B}}T},\quad \xi=\frac{mB}{k_{\mathrm{B}}T}. \tag{D1}$$

Thus, when the bias field is applied along the anisotropy axis ($\vec{B}\|\hat{n}$), the equilibrium probability distribution for $z=(\vec{m}/m)\cdot\hat{n}$, associated with the Hamiltonian (3.1) (in the absence of the probing field), reads

$$P_0(z)=\frac{1}{\mathcal{Z}}e^{-\beta\mathcal{H}(z)},\quad -\beta\mathcal{H}(z)=\sigma z^2+\xi z, \tag{D2}$$

where $\mathcal{Z}=\int_{-1}^{1}dz\,\exp(\sigma z^2+\xi z)$ is the partition function. This can be written in terms of the Dawson integral $D(x)$ (Ref. 40, p. 298), $\sigma_{\pm}=\sigma(1\pm h)^2$, and $h=B/B_K=\xi/2\sigma$, as

$$\mathcal{Z}(\sigma,\xi)=\frac{e^{\sigma}}{\sqrt{\sigma}}[e^{\xi}D(\sqrt{\sigma_+})+e^{-\xi}D(\sqrt{\sigma_-})] \tag{D3}$$

[in order to compute $D(x)$ we employ the subroutine DAWSON of Ref. 38, p. 252]. The equilibrium averages with respect to $P_0(z)$ will be denoted by $\langle\rangle_0$.

On introducing the equilibrium average of the nth Legendre polynomial $p_n(z)$ [$p_1(z)=z$, $p_2(z)=\frac{1}{2}(3z^2-1)$, ...], namely, $S_n(\sigma,\xi)=\int_{-1}^{1}dz\,p_n(z)P_0(z)$, and accounting for the expression for the equilibrium susceptibility tensor [cf. Eq. (C13)] $\chi_{ij}=(\mu_0/k_{\mathrm{B}}T)[\langle m_i m_j\rangle_0-\langle m_i\rangle_0\langle m_j\rangle_0]$, the longitudinal, $\chi_{\|}=\chi_{zz}$, and transverse, $\chi_{\perp}=\chi_{xx}=\chi_{yy}$, susceptibilities for a spin with a general axially symmetric Hamiltonian $\mathcal{H}(z)$ can be written as

$$\chi_{\|}=\frac{\mu_0 m^2}{k_{\mathrm{B}}T}\left(\frac{1+2S_2}{3}-S_1^2\right),\quad \chi_{\perp}=\frac{\mu_0 m^2}{k_{\mathrm{B}}T}\,\frac{1-S_2}{3}, \tag{D4}$$

where we have used $\langle m_z\rangle_0=mS_1$, $\langle m_z^2\rangle_0=m^2\frac{1}{3}(1+2S_2)$, $\langle m_{x,y}\rangle_0=0$, and $\langle m_{x,y}^2\rangle_0=\frac{1}{2}(m^2-\langle m_z^2\rangle_0)$. For $-\beta\mathcal{H}(z)=\sigma z^2+\xi z$, S_1 and S_2 are explicitly given by (see Refs. 41,31):

$$S_1=\frac{e^{\sigma}}{\sigma\mathcal{Z}}\sinh\xi-h, \tag{D5}$$

$$S_2=\frac{3}{2}\left[\frac{e^{\sigma}}{\sigma\mathcal{Z}}(\cosh\xi-h\sinh\xi)+h^2-\frac{1}{2\sigma}\right]-\frac{1}{2}. \tag{D6}$$

On the other hand, on applying $S_1=\mathcal{Z}^{-1}\partial\mathcal{Z}/\partial\xi$ and $(1+2S_2)/3=\mathcal{Z}^{-1}\partial\mathcal{Z}/\partial\sigma$ to the approximate $\mathcal{Z}$ obtained by introducing in Eq. (D3) the leading term in the asymptotic expansion of the Dawson integral, $D(x)\simeq 1/2x$, one gets the following high-barrier ($\sigma\gg 1$, $h=\xi/2\sigma\ll 1$) approximations of Eqs. (D4)

$$\chi_{\|}\simeq\frac{\mu_0 m^2}{k_{\mathrm{B}}T}\,\frac{1}{(\cosh\xi-h\sinh\xi)^2}\left\{(1-h^2)-\frac{1}{\sigma}+\frac{1}{8\sigma^2}\left[1-\frac{1+6h^2+h^4}{(1-h^2)^2}\cosh(2\xi)+\frac{4h(1+h^2)}{(1-h^2)^2}\sinh(2\xi)\right]\right\}, \tag{D7}$$

$$\chi_{\perp}\simeq\frac{\mu_0 m^2}{k_{\mathrm{B}}T}\,\frac{1}{2\sigma}\,\frac{(1+h^2)\cosh\xi-2h\sinh\xi}{(1-h^2)(\cosh\xi-h\sinh\xi)}. \tag{D8}$$

Furthermore, on taking formally the $K\to\infty$ limit in these formulas (i.e., $\sigma\to\infty$ and $h=\xi/2\sigma\to 0$), one gets the ''Ising-type'' equilibrium susceptibilities

$$\chi_{\|}\simeq\frac{\mu_0 m^2}{k_{\mathrm{B}}T}\,\frac{1}{\cosh^2\xi},\quad \chi_{\perp}\simeq 0. \tag{D9}$$

2. Linear dynamic susceptibility

When the probing field points along an arbitrary direction α with respect to the anisotropy axis, the effective susceptibility is given by $\chi=\chi_{\|}\cos^2\alpha+\chi_{\perp}\sin^2\alpha$. Shliomis and Stepanov[23] (see also Ref. 42) proposed a simple two Debye form for $\chi(\omega)$, which can be generalized in order to describe the effect of a longitudinal bias field by writing

$$\chi_{\mathrm{ShS}}=\frac{\chi_{\|}(T,B)}{1+i\omega\tau_{\|}}\cos^2\alpha+\frac{\chi_{\perp}(T,B)}{1+i\omega\tau_{\perp}}\sin^2\alpha, \tag{D10}$$

where $\tau_{\|}$ and $\tau_{\perp}$ are appropriate longitudinal and transverse relaxation times (see below).

In the main text Eq. (D10) [with the exact equilibrium susceptibilities (D4)] is referred to as the Shliomis and Stepanov equation. On the other hand, the formula obtained when in Eq. (D10) one puts $\tau_{\perp}=0$ (instantaneous transverse response) and uses the high-barrier approximations (D7) and (D8), is called the Gittleman, Abeles, and Bozowski equation, since it properly generalizes their formula[43] to $B\neq 0$ and an arbitrary anisotropy-axis orientation. In fact, on introducing Eqs. (D7) and (D8) evaluated at $B=0$ in Eq. (D10) and setting $\tau_{\perp}=0$, one first gets

$$\chi_{\mathrm{GAB}}\simeq\left[\frac{\mu_0 m^2}{k_{\mathrm{B}}T}\cos^2\alpha+\frac{\mu_0 m^2}{Kv}\left(\tfrac{3}{2}\sin^2\alpha-1\right)+i\omega\tau_{\|}\,\frac{\mu_0 m^2}{2Kv}\sin^2\alpha\right]\frac{1}{1+i\omega\tau_{\|}}, \tag{D11}$$

which, when averaged over an ensemble with randomly distributed anisotropy axes, reduces to the equation proposed in

Ref. 43. Finally, the expression obtained when one introduces the Ising-type Eqs. (D9) into Eq. (D10), namely

$$\chi_{\rm Ising}=\frac{\mu_0 m^2}{k_{\rm B}T}\,\frac{1}{\cosh^2\xi}\,\frac{\cos^2\alpha}{1+i\omega\tau_{\parallel}}, \tag{D12}$$

is called the discrete-orientation dynamic susceptibility.

3. Relaxation times

For the relaxation times in the above formulas a number of expressions can be used.

a. Longitudinal relaxation time

The response to a longitudinal static probing field is given by the time-domain counterpart of Eq. (4.1), namely, $\chi_{\parallel}\Sigma_{k=1}^{\infty}a_k\exp(-\Lambda_k t)$, where a_k $(\Sigma_{k\geqslant 1}a_k=1)$ is the amplitude corresponding to the eigenvalue Λ_k of the Sturm-Liouville equation associated with the Fokker-Planck equation $(0=\Lambda_0<\Lambda_1\leqslant\Lambda_2\cdots)$. The first nonvanishing eigenvalue Λ_1 is related with inter-potential-well dynamics, while the information about the intra-potential-well relaxation appears in the higher-order eigenvalues Λ_k, $k\geqslant 2$. In some cases, however, Λ_1 corresponds to a ''long-lived'' mode and characterizes reasonably well the relaxation (except for the earliest stages). The approximate expressions for Λ_1^{-1} derived by Brown[2] are

$$\tau_{\parallel}\simeq\begin{cases}\tau_{\rm N}\left[1-\dfrac{2}{5}\sigma+\dfrac{48}{875}\sigma^2\left(1+\dfrac{175}{24}h^2\right)\right]^{-1}, & \sigma\ll 1,\\[2ex] \tau_{\rm N}\dfrac{\sqrt{\pi}}{2}\sigma^{-3/2}\dfrac{\exp[\sigma(1+h^2)]}{(1-h^2)(\cosh\xi-h\sinh\xi)}, & \sigma\gg 1,\end{cases}$$

where we have written $\tau_{\parallel}=\Lambda_1^{-1}$ and $\tau_{\rm N}$ is given by Eq. (2.6).

Nevertheless, when the relaxation comprises different decay modes, a more useful definition of the thermoactivation rate is that of *integral relaxation time* $\tau_{{\rm int},\parallel}$, which is the area enclosed by the relaxation curve (normalized at $t=0$) after a sudden infinitesimal change at $t=0$ of the external field. On employing this definition, Garanin, Ishchenko, and Panina[21] obtained the following formula for *any* axially symmetric Hamiltonian $\mathcal{H}(z)$ (see also Refs. 44,45)

$$\tau_{{\rm int},\parallel}=\frac{2\tau_{\rm N}}{\partial\langle z\rangle_0/\partial\xi}\int_{-1}^{1}\frac{dz}{1-z^2}[\Phi(z)]^2[P_0(z)]^{-1}, \tag{D13}$$

where $\Phi(z)$, for which explicit expressions can be derived for special forms of $\mathcal{H}(z)$, is in general given by $\Phi(z)=\int_{-1}^{z}dz_1P_0(z_1)[\langle z\rangle_0-z_1]$. In the unbiased case, the integral relaxation time yields the results for Λ_1^{-1} of Brown in the appropriate limiting cases.[21,44] However, $\tau_{{\rm int},\parallel}$ depends on the whole set of eigenvalues, $\tau_{{\rm int},\parallel}=\Sigma_{k\geqslant 1}a_k\Lambda_k^{-1}$, and hence is more informative than Λ_1^{-1}.

b. Transverse relaxation time

The expression usually considered for the transverse relaxation time is that yielded by the effective eigenvalue (moment) method (see, e.g., Ref. 46),

$$\tau_{\perp}^{\rm od}=2\tau_{\rm N}\frac{1-S_2(\sigma,\xi)}{2+S_2(\sigma,\xi)}. \tag{D14}$$

Nevertheless, this formula does not account for gyromagnetic effects and holds in the overdamped $(\lambda\gg 1)$ case only.

Raĭkher and Shliomis[29,30] studied effects of the gyromagnetic terms on the transverse response by a decoupling ansatz for the infinite system of differential equations for the averages of the magnetic moment [recall the remarks after Eqs. (2.9) and (2.10)]. An expression for $\chi_{\perp}(\omega)|_{B=0}$ was derived, which can be written as

$$\chi_{\perp}(\omega,T)=\chi_{\perp}(T)\frac{1+i\omega 2\tau_{\rm N}\dfrac{\lambda_a}{\lambda_a\lambda_b+\lambda_c}}{1-4\omega^2\tau_{\rm N}^2\dfrac{1}{\lambda_a\lambda_b+\lambda_c}+i\omega 2\tau_{\rm N}\dfrac{\lambda_a+\lambda_b}{\lambda_a\lambda_b+\lambda_c}},$$

where $\chi_{\perp}(T)$ is the equilibrium transverse susceptibility and $[S_2^0=S_2(\sigma,\xi)|_{\xi=0}]$

$$\lambda_a=\frac{2+S_2^0}{1-S_2^0},\quad \lambda_b=\frac{2\sigma}{3}\,\frac{2+S_2^0\left(1-\dfrac{6}{\sigma}\right)}{S_2^0},\quad \lambda_c=\frac{1}{\lambda^2}\,\frac{6\sigma S_2^0}{1-S_2^0}.$$

In the low-frequency range, the above $\chi_{\perp}(\omega)$ can be expanded in powers of $\omega\tau_{\rm N}$ (to first order), and then cast into the form of a Debye-type formula by using $1-\epsilon x\simeq(1+x)^{-\epsilon}$, namely,

$$\chi_{\perp}(\omega,T)\simeq\chi_{\perp}(T)\frac{1}{1+i\omega 2\tau_{\rm N}\dfrac{\lambda_b}{\lambda_a\lambda_b+\lambda_c}}.$$

Accordingly, the quantity multiplying $i\omega$ defines an effective relaxation time that can be written as

$$\tau_{\perp}|_{\xi=0}=2\tau_{\rm N}\frac{1-S_2^0}{2+S_2^0}\,\frac{1}{1+p(\sigma)/\lambda^2}, \tag{D15}$$

where

$$p(\sigma)=\frac{(3S_2^0)^2}{(2+S_2^0)[2+S_2^0(1-6/\sigma)]}. \tag{D16}$$

Note that, in the absence of the gyromagnetic terms $(\lambda\to\infty)$, Eq. (D15) reduces to the unbiased case of the overdamped result (D14).

*Electronic address: jlgarcia@posta.unizar.es

[1] L. Néel, Ann. Geophys. **5**, 99 (1949).
[2] W. F. Brown, Jr., Phys. Rev. **130**, 1677 (1963).
[3] R. Kubo and N. Hashitsume, Prog. Theor. Phys. Suppl. **46**, 210 (1970).
[4] R. Ettelaie and M. A. Moore, J. Phys. A **17**, 3505 (1984).
[5] K. Binder and D. Stauffer, in *Applications of the Monte Carlo Method in Statistical Physics*, edited by K. Binder (Springer,

Berlin, 1984), p. 1.
[6] D. Rodé, H. N. Bertram, and D. R. Fredkin, IEEE Trans. Magn. **MAG-23**, 2224 (1987).
[7] A. Aharoni, Phys. Rev. **135**, A447 (1964).
[8] L. Bessais, L. Ben Jaffel, and J. L. Dormann, Phys. Rev. B **45**, 7805 (1992).
[9] W. T. Coffey, D. S. F. Crothers, Y. P. Kalmykov, E. S. Massawe, and J. T. Waldron, Phys. Rev. E **49**, 1869 (1994).
[10] Y. L. Raĭkher and V. I. Stepanov, Phys. Rev. B **52**, 3493 (1995).
[11] W. T. Coffey, D. S. F. Crothers, Y. P. Kalmykov, and J. T. Waldron, Phys. Rev. B **51**, 15 947 (1995).
[12] A. Lyberatos, D. V. Berkov, and R. W. Chantrell, J. Phys.: Condens. Matter **5**, 8911 (1993).
[13] A. Lyberatos and R. W. Chantrell, J. Appl. Phys. **73**, 6501 (1993).
[14] W. Wernsdorfer, E. Bonet Orozco, K. Hasselbach, A. Benoit, B. Barbara, N. Demoncy, A. Loiseau, H. Pascard, and D. Mailly, Phys. Rev. Lett. **78**, 1791 (1997).
[15] W. F. Brown, Jr., J. Appl. Phys. **30**, 130s (1959).
[16] M. I. Shliomis and V. I. Stepanov, Adv. Chem. Phys. **87**, 1 (1994).
[17] P. Svedlindh, T. Jonsson, and J. L. García-Palacios, J. Magn. Magn. Mater. **169**, 323 (1997).
[18] N. G. van Kampen, *Stochastic Processes in Physics and Chemistry* (North-Holland, Amsterdam, 1981).
[19] H. Risken, *The Fokker-Planck Equation*, 2nd ed. (Springer, Berlin, 1989).
[20] D. A. Garanin, Phys. Rev. B **55**, 3050 (1997).
[21] D. A. Garanin, V. V. Ishchenko, and L. V. Panina, Theor. Math. Phys. (USSR) **82**, 169 (1990) [Teor. Mat. Fiz. **82**, 242 (1990)].
[22] V. V. Shcherbakova, Izvestiya, Earth Phys. **14**, 308 (1978).
[23] M. I. Shliomis and V. I. Stepanov, J. Magn. Magn. Mater. **122**, 176 (1993).
[24] W. T. Coffey, D. S. F. Crothers, Y. P. Kalmykov, and J. T. Waldron, Physica A **213**, 551 (1995).
[25] P. J. Cregg, D. S. F. Crothers, and A. W. Wickstead, J. Appl. Phys. **76**, 4900 (1994).
[26] B. A. Storonkin, Sov. Phys. Crystallogr. **30**, 489 (1985) [Kristallografiya **30**, 841 (1985)].
[27] W. F. Brown, Jr., IEEE Trans. Magn. **MAG-15**, 1196 (1979).
[28] M. Morillo and J. Gómez-Ordóñez, Phys. Rev. Lett. **71**, 9 (1993).
[29] Y. I. Raĭkher and M. I. Shliomis, Sov. Phys. JETP **40**, 526 (1975) [Zh. Eksp. Teor. Fiz. **67**, 1060 (1974)].
[30] Y. L. Raĭkher and M. I. Shliomis, Adv. Chem. Phys. **87**, 595 (1994).
[31] Y. P. Kalmykov and W. T. Coffey, Phys. Rev. B **56**, 3325 (1997).
[32] A.-L. Barra, P. Debrunner, D. Gatteschi, C. E. Schultz, and R. Sessoli, Europhys. Lett. **35**, 133 (1996).
[33] A. M. Gomes, M. A. Novak, R. Sessoli, A. Caneschi, and D. Gatteschi, Phys. Rev. B **57**, 5021 (1998).
[34] P. E. Kloeden and E. Platen, *Numerical Solution of Stochastic Differential Equations* (Springer, Berlin, 1995), 2nd corr. printing.
[35] W. Rümelin, SIAM (Soc. Ind. Appl. Math.) J. Numer. Anal. **19**, 604 (1982).
[36] Y. Nakatani, Y. Uesaka, N. Hayashi, and H. Fukushima, J. Magn. Magn. Mater. **168**, 347 (1997).
[37] V. P. Antropov, S. V. Tretyakov, and B. N. Harmon, J. Appl. Phys. **81**, 3961 (1997).
[38] W. H. Press, S. A. Teukolsky, W. T. Vetterling, and B. P. Flannery, *Numerical Recipes*, 2nd ed. (Cambridge University Press, New York, 1992).
[39] A. Greiner, W. Strittmatter, and J. Honerkamp, J. Stat. Phys. **51**, 95 (1988).
[40] M. Abramowitz and I. A. Stegun, *Handbook of Mathematical Functions* (Dover, New York, 1964).
[41] F. G. West, J. Appl. Phys. **32**, 249s (1961).
[42] Y. L. Raĭkher and V. I. Stepanov, Phys. Rev. B **55**, 15 005 (1997).
[43] J. I. Gittleman, B. Abeles, and S. Bozowski, Phys. Rev. B **9**, 3891 (1974).
[44] D. A. Garanin, Phys. Rev. E **54**, 3250 (1996).
[45] W. T. Coffey and D. S. F. Crothers, Phys. Rev. E **54**, 4768 (1996).
[46] W. T. Coffey, Y. P. Kalmykov, and E. S. Massawe, Adv. Chem. Phys. **85**, 667 (1993), (part 2).